Westfälische
Wilhelms-Universität
Münster

Charmonium production cross sections with PYTHIA at LHC energies

Bachelor Thesis

Nicolas Tiltmann

Westfälische Wilhelms-Universität Münster
Institut für Kernphysik
AG Andronic / Klein-Bösing

First Referee: Prof. Dr. Anton Andronic
Second Referee: apl. Prof. Dr. Christian Klein-Bösing

Münster, October 2020

Declaration of Academic Integrity

I, *Nicolas Tiltmann*, hereby confirm that this thesis on "Charmonium production cross sections with PYTHIA at LHC energies" is solely my own work and that I have used no sources or aids other than the ones stated. All passages in my thesis for which other sources, including electronic media, have been used, be it direct quotes or content references, have been acknowledged as such and the sources cited.

Münster, 05. October 2020

Nicolas Tiltmann

I agree to have my thesis checked in order to rule out potential similarities with other works and to have my thesis stored in a database for this purpose.

Münster, 05. October 2020

Nicolas Tiltmann

Contents

1 Introduction

Charmonium is a bound state of a charm quark and an anti-charm quark which can form in high energy particle collisions. The production of such particles is dependent on especially the transverse momentum (p_T) and can be quantified and measured as cross section σ in proton-proton (pp) collisions. This is an essential step to the understanding of proton-nucleus and nucleus-nucleus collision which then can be used to further investigate the quark-gluon plasma (QGP) [Ach+17].

Quarks and gluons have a particle property called colour charge. In regular matter, only particles with a total colour of white can be observed. This can either be achieved trough combination of the three different colours, red, blue and green, a combination of the three anticolours or a combination of a colour with its corresponding anticolour. This phenomenon is called confinement [Dem17]. Under extreme energy densities a quark-gluon plasma can from in which a deconfinement of the colour charges can be observed.

In proton-lead collisions, a change of charmonium production cross sections with respect to pp collisions could be measured. For the investigation of the quark-gluon plasma in Pb-Pb collisions, it is important to know whether the modified charmonium production is a direct consequence of the QGP or if it originates from another effect. Therefore, a good understanding of charmonium production itself is crucial [Aab+18].

Particle collision experiments like ALICE (A Large Ion Collider Experiment) located at the CERN Large Hadron Collider (LHC) offer the possibility to measure charmonium production cross sections in high energy proton-proton collisions. On the other hand, Monte Carlo event generators can simulate the same kind of particle collisions using an implemented physics model. It is possible to calculate the same kind of charmonium production cross sections based on the simulated events and the compare it to measurements.

PYTHIA is a Monte Carlo event generator for pp and other collisions written by *Torbjörn Sjöstrand et al.* [Sjö+15]. The PYTHIA program itself is tuned with experimental results from particle collision experiments. However, the used *Monash 2013 Tune* [SCR14] existed before any particle collider achieved centre-of-mass energies of $\sqrt{s} = 13\,\mathrm{TeV}$. This means, that the tune could not have been fed with such data. The comparison of simulated cross sections with measurements may reveal if a further tune is needed to describe charmonium production at $\sqrt{s} = 13\,\text{TeV}$ correctly.

Here, this comparison between experimental measurements and simulated results is done to evaluate the charmonium production simulation capabilities of the PYTHIA event generator. In this thesis, the cross sections for J/ψ production in pp collisions at a centre-of-mass energy of $\sqrt{s} = 5.02\,\text{TeV}$ and $\sqrt{s} = 13\,\text{TeV}$ as well as the $\psi(2\mathrm{S})$ cross sections at $\sqrt{s} = 13\,\text{TeV}$ calculated by PYTHIA are compared with several datasets of ALICE, ATLAS and LHCb experiments. For J/ψ, a differentiation between prompt and non-prompt production is done.

Finally, a comparison of $b\bar{b}$-pair production cross section between PYTHIA simulated and FONLL calculated results is done in order to understand the process of non-prompt J/ψ production.

2 Theoretical Background

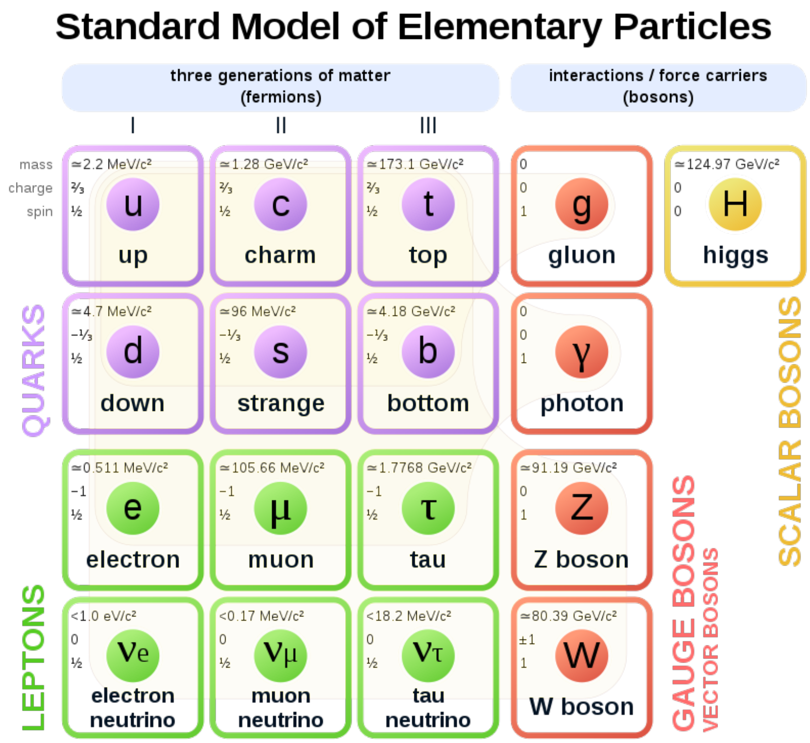

Figure 2.1: The standard model of particle physics. Taken from [Mis19].

The standard model of particle physics contains a total of six quarks, six leptons and five bosons. An overview is given in figure 2.1. Quarks interact via all fundamental forces: strong and weak interaction, electromagnetic interaction and gravity. There are six quarks: up (u), down (d), strange (s), charm (c), bottom (b) and top (t). The latter three are significantly more massive than the first three. This is important for the production of quarkonium which will be discussed later. The leptons consist of the electron e, the muon μ, and the tau τ as well as the electron neutrino ν_e, the muon neutrino ν_μ and the tau neutrino ν_τ. The first three interact via the weak and electromagnetic interaction and gravity. The neutrinos have no electric charge and therefore only interact via weak interaction and gravity. The gauge bosons gluon (g), photon (γ), Z and W are the particles that carry the fundamental forces with exception of gravity, which could not yet be integrated into the standard model. The

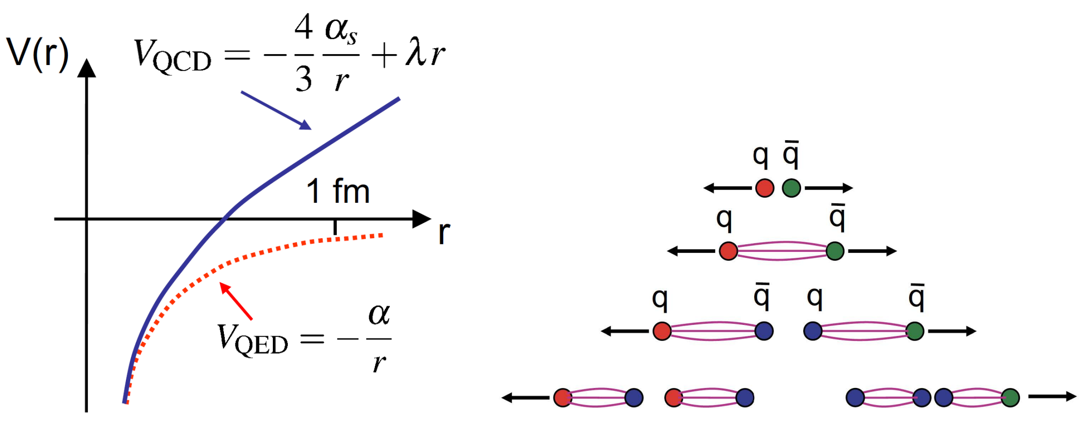

(a) QCD and QED potential (b) Confinement

Figure 2.2: (a) Potentials of strong interaction described by quantum chromodynamics (QCD) and electromagnetic interaction described by quantum electrodynamics (QED) (b) String breaking in mesons and the resulting confinement. Both taken from [Tho09].

Higgs boson (H) was detected at CERN in 2012. Additionally, an antiparticle for every particle exists. For antiparticles, the sign of every charge is flipped, while all other physical properties, such as the mass, are unchanged. The antiparticle of an electron e^- with charge $-e$ is the positron e^+ with the charge $+e$. In case of the quarks, the anti-particles also carry the respective anticolours, for example anti-blue [Dem17].

2.1 The Strong Interaction

The strong interaction is described by quantum chromodynamics (QCD) and causes a force between particles with a colour charge. This affects quarks and gluons. The colour charges follow a SU(3) symmetry and therefore the strong interaction is invariant under rotation of the colours. The colour charge of a quark is always a colour and an antiquark always has an anticolour. The gluons always carry a colour *and* an anticolour. However, the observable states of gluons are superpositions of the single colour states. In contrast to the electromagnetic force with the electrical charge, the strong force does not only have an attractive $1/r$-behaviour. The QCD potential is given by [Tho09]

$$V_{\mathrm{QCD}} = -\frac{4}{3}\frac{\alpha_{\mathrm{s}}}{r} + \lambda r, \tag{2.1}$$

where α_{s} is the coupling constant of the strong interaction and r the distance fo colour charged particles. λ is the string tension with a value of $\lambda \approx 1\,\mathrm{GeV\,fm^{-1}}$. The potential energy rises with $1/r$ for small distances just as in electromagnetic interaction[1], but for

[1] described by quantum electrodynamics (QED)

larger distances the behaviour changes into a linear increase. This is shown in figure 2.2a. If one tries to separate particles bound by strong the force, the potential energy of the binding increases approximately linearly at larger distances. At some point, the potential energy is large enough to create a new quark-antiquark pair. This process can be seen in figure 2.2b. The colour charges get neutralised again by their respective anticolour. Therefore, colour charges can never be observed independently on larger scales. This is called confinement [Tho09; Dem17].

2.2 Quarkonium

Quarkonia are mesons consisting of a quark and its corresponding antiquark. Therefore, a quarkonium is its own antiparticle. The three light quarks, up (u), down (d) and strange (s) do not form quarkonium due to their relatively small mass difference. However, the observable states of light quark mesons can be superpositions of the single flavour states. This can for example be the pion π^0, which is a superposition of $u\bar{u}$ and $d\bar{d}$ [Dem17]. The heavier quarks, charm (c) and bottom (b), form well defined mesons of quark and antiquark without superposition. They are called charmonium ($c\bar{c}$) and bottomonium ($b\bar{b}$). The top quark (t) can not form quarkonium due to its short lifetime [Pov+14].

2.2.1 Charmonium

The most frequently observed state of charmonium is the J/ψ particle. It was discovered in 1974 by *Burton Richter et al.* at the SLAC and *Samuel Ting et al.* at BNL independently. The J/ψ was the first particle observed that contains one of the heavy quarks. The J/ψ has a rest mass of $(3096.900 \pm 0.006)\,\mathrm{MeV}$ [Tan+18] and a mean lifetime of $(7.1 \pm 0.3) \times 10^{-21}\,\mathrm{s}$ [Tan+18]. The main decay mode produces hadronic final states via either strong or electromagnetic interaction. It occurs with a probability of $(87.7 \pm 0.5)\%$. Furthermore, there are the dielectronic decay $\mathrm{J}/\psi \to e^+e^-$ with a probability of $(5.971 \pm 0.032)\%$ and the dimuonic decay $\mathrm{J}/\psi \to \mu^+\mu^-$ which occurs in $(5.961 \pm 0.033)\%$ percent of the cases [Tan+18].

J/ψ mesons can be divided in two major categories regarding their origin. Prompt J/ψ are produced either directly in a pp collision or trough the decay of excited charmonium states, for example $\psi(2\mathrm{S})$. On the other hand, non-prompt J/ψ originate in the decay of bottom flavoured hadrons (B-hadrons). The B^0 meson ($d\bar{b}$) has a mean lifetime of $1.5 \times 10^{-12}\,\mathrm{s}$ [Tan+18]. This is about 9 orders of magnitude longer than for example the lifetime of the decay $\psi(2\mathrm{S}) \to \mathrm{J}/\psi$ and therefore, the J/ψ produced in b-hadron decays are called non-prompt. The cross section of prompt and non-prompt J/ψ combined is called inclusive cross section.

The first exited state of J/ψ is $\psi(2S)$. It has a rest mass of (3686.09 ± 0.04) MeV [Tan+18] and a mean lifetime of $(2.2 \pm 0.1) \times 10^{-21}$ s [Tan+18]. Compared to J/ψ, the $\psi(2S)$ is slightly more massive and decays slightly faster. In this case, $(97.85 \pm 0.13)\%$ of the decays are hadronic. $(61.4 \pm 0.6)\%$ of the decays include the charmonium ground state J/ψ as final particle. The direct dileptonic decays of $\psi(2S)$ occur very rarely. The probability for dielectronic decay is $(0.793 \pm 0.017)\,\%$ and for the dimuonic decay $(0.80 \pm 0.06)\,\%$. Additionally, the decay into two taus, $\psi(2S) \to \tau^+\tau^-$, can be observed with a probability of $(0.31 \pm 0.04)\,\%$ [Tan+18].

2.2.2 Bottomonium

Bottomonia are the quarkonia built from bottom quarks. The most prominent type is the $\Upsilon(1S)$ particle. It has a rest mass of (9460.30 ± 0.26) MeV [Tan+18] which is about three times higher than the rest mass of J/ψ. It has a mean lifetime of $(1.22 \pm 0.03) \times 10^{-20}$ s [Tan+18]. This is about double as long as the J/ψ. Bottomonia can decay into charmonia, for example J/ψ. The probability for a process containing a J/ψ as a final state is $(0.054 \pm 0.004)\,\%$ [Tan+18].

2.3 Kinematic Variables

To characterise pp collisions, three kinematic variables are sufficient. There are many more variables like the azimuthal angle ϕ between the particle and the x axis, but the case of pp collisions is rotationally symmetric, so the physics does not depend on this angle. Furthermore, natural units are used, so $\hbar = c = 1$. Energy, momentum and mass are all given in units of eV.

First, there is the total energy in the collision process. Usually, this is given as the centre-of-mass energy $\sqrt{s}$. Every particle in the event can be described trough its transverse momentum p_T and its rapidity y or pseudorapidity η. The transverse momentum p_T is defined as the fraction of the momentum orthogonal to the beam axis. In terms of the ALICE coordinate system from figure 3.2, it is the projection of the total momentum on the xy-plane. A calculation is possible via

$$p_\mathrm{T} = |\vec{p}| \sin\theta, \tag{2.2}$$

where $\vec{p}$ is the total momentum and θ the polar angle between the particle and the beam axis according to figure 3.2. The rapidity is defined as

$$y = \frac{1}{2} \ln \frac{E + p_\mathrm{z}}{E - p_\mathrm{z}} \tag{2.3}$$

with the energy E and the momentum parallel to the beam axis p_z. The rapidity is additive under Lorentz transformation. However, in experiments, the mass of a particle is often difficult to measure. The pseudorapidity is more easy to measure. It is defined as

$$\eta = -\ln \tan \frac{\theta}{2} \tag{2.4}$$

and only depends on the polar angle θ. In high-energy physics, one can use the approximation

$$\eta \approx y \tag{2.5}$$

which is suitable if $m \ll |\vec{p}|$, where m is the rest mass of the particle and $|\vec{p}|$ the magnitude of the momentum [SR11].

2.4 $b\bar{b}$-Pair Production with the FONLL Framework

The Fixed-Order Next-to-Leading Logarithm (FONLL) framework provides a possibility to calculate heavy quark production cross sections in a theoretical framework [CGN98; Cac+12]. There is a free online tool by *Matteo Cacciari* available at `http://www.lpthe.jussieu.fr/~cacciari/fonll/fonllform.html` to calculate those cross sections. The cross sections for bottom quarks is then calculated by the website to compare it to PYTHIA simulations and achieve an insight into the non-prompt J/ψ production via the b-quark decay. The output of the FONLL website also includes the uncertainties of the calculated cross sections.

3 Experimental Approach

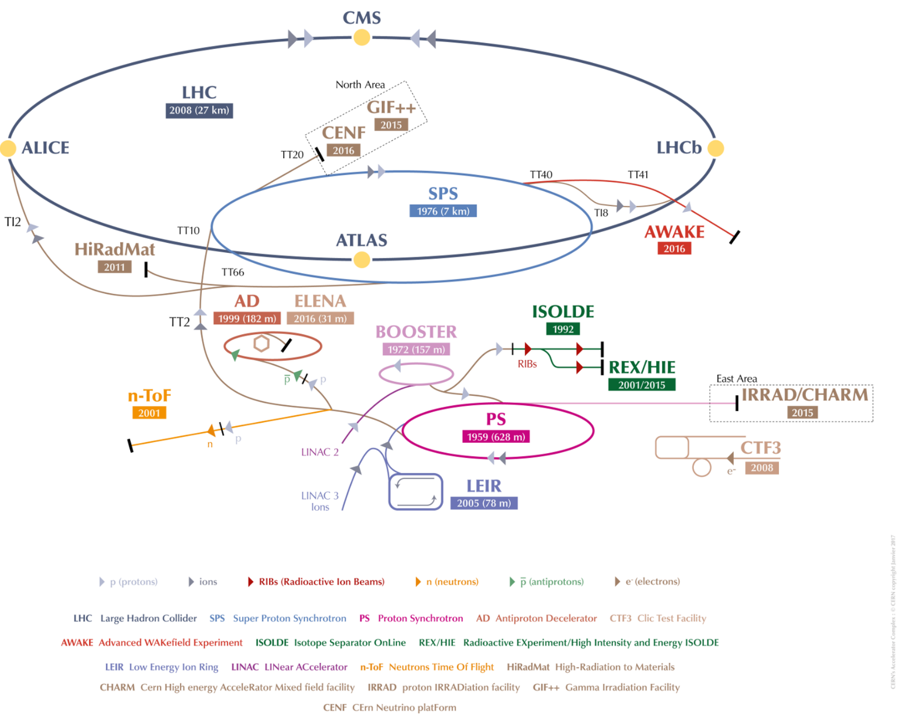

Figure 3.1: Schematic view of the CERN facilities and accelerators. Taken from [Mob16].

The Large Hadron Collider (LHC) is located at European Organization for Nuclear Research (french: *Organisation européenne pour la recherche nucléaire*, acronym: CERN) in Switzerland and France and it is the currently largest particle accelerator for protons and lead-ions. First data has been collected in 2007. A schematic overview of the CERN accelerator complex is given in figure 3.1, where the LHC is marked in dark blue. The accelerator itself is a synchrotron located in a 27 km long tunnel. The accelerator is fed with a row of pre-accelerators. For protons, these are: Linac2, PS Booster, Proton Synchrotron and Super Proton Synchrotron. The first is a linear accelerator while the latter ones are synchrotrons. The path of the protons can be traced using the small, light grey arrows in figure 3.1. In the LHC, one beam of protons is accelerated clockwise and the other one counterclockwise. With

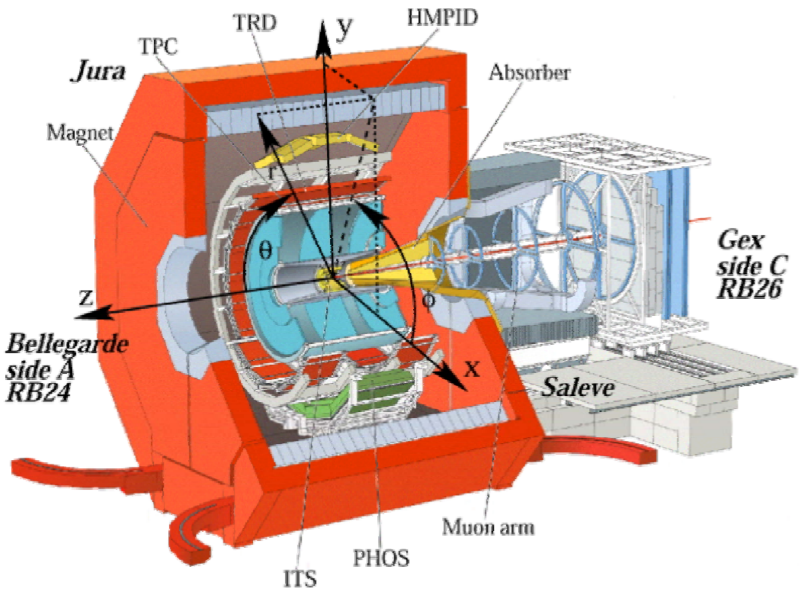

Figure 3.2: Schematic view of the ALICE detector. The axes x, y, z and the angles θ and ϕ define the coordinate system used in this entire work. Taken from [BC03, p. 3, fig. 1]

a kinetic energy of 6.5 TeV per proton this results in a centre-of-mass energy of 13 TeV at the interaction points. There are four points where the two beam pipes intersect and protons collide. Around these points four large detectors are installed: ATLAS, ALICE, LHCb and CMS [CER17]. By 2027 the LHC will be upgraded to High-Luminosity LHC featuring a 10 times higher peak luminosity with respect to the design peak luminosity of the LHC. This will increase the number of interactions significantly [CER20].

3.1 ALICE

The ALICE (A Large Ion Collider Experiment) experiment is mainly designed for the study of lead-lead collisions. At the high temperatures and energy densities quark-gluon plasma can form. The detector also collects data at proton-proton collisions to study for example the charmonium production. Figure 3.2 gives a schematic overview over its components. The central detector consists of different types of subdetectors layered concentrically around the interaction point. All the cylindrical detectors lie within a large solenoid (red) which generates a magnetic field of 0.5 T. From inside to outside these are the Inner Tracking System (ITS, yellow), Time Projection Chamber (TPC, blue), Transition Radiation Detector (TRD, red) and Time Of Flight (TOF, not shown, directly around TRD). They all offer a full 360° azimuthal angle coverage and a pseudorapidity acceptance of at least $|\eta| \leq 0.84$. At different positions around the beam axis there are some more detectors, such as calorimeters, placed. In negative z-direction the Muon Spectrometer (yellow, blue and grey cone at the right side) is placed. It is capable of detecting muons with pseudorapidity $-4 \leq \eta \leq -2.5$ at any azimuthal angle. J/ψ particles can be detected in either the dielectron or dimuon decay channel. In case of the dielectron channel the ITS and TPC are the most relevant detectors and for the dimuon channel it is the Muon Spectrometer [Aam+08].

3.1.1 The Tracking Detectors ITS and TPC

The Inner Tracking System (ITS) is made up by silicon semiconductor detectors arranged in different shapes and six individual layers. The innermost two layers are Silicon Pixel Detectors (SPD), followed by two Silicon Drift Detectors (SDD). The ITS is finished by two layers of Silicon Strip Detectors (SSD). While the SPD outputs only a binary signal for trajectory determination, the SDD and SSD can additionally be used for particle identification via energy loss $\mathrm{d}E/\mathrm{d}x$ in low-p_{T} ranges. The next layer is the Time Projection Chamber (TPC), a multi-wire proportional chamber (MWPC). The detector is filled with $90\,\mathrm{m}^3$ of $\mathrm{Ne/CO_2/N_2}$ gas. Charged particles flying through the TPC ionise the gas and a high voltage of $100\,\mathrm{kV}$ separates the ions and electrons. The collected charge is proportional to the particle energy. This also allows particle identification via energy loss $\mathrm{d}E/\mathrm{d}x$ but at higher p_{T} than the ITS. The ITS and TPC have a pseudorapidity acceptance of at least $|\eta| < 0.9$. These layers together enable a reconstruction of the particles trajectories. Due to the magnetic field and Lorentz force the charged particles have a curved trajectory. Using the radius of curvature it is possible to calculate the momenta of charged particles. This way, the electron and positron originating from a J/ψ decay can be detected in the given pseudorapidity range [Aam+08].

3.1.2 The Muon Spectrometer

The Muon Spectrometer (see figure 3.3) was specifically designed for the detection of charmonia and bottomonia like J/ψ, $\psi(2S)$ and Υ. It is placed around the beam pipe (red) in negative z-direction and it covers a pseudorapidity range of $-4 \leq \eta \leq -2.5$. This corresponds to a polar angle of roughly $171° - 178°$ with respect to the point of interaction. The azimuthal angle range is fully covered. Starting from the point of interaction, the first part is an absorber (grey) made of carbon and concrete. Only high-momentum muons are able to pass this absorber. Muons that passed the absorber are tracked by 10 detection layers (light blue) in a $0.7\,\mathrm{T}$ magnetic field (dipole magnet in pink). The detection layers are combined in groups of two. Each detection layer is a single cathode pad chamber, a gas detector, where every cathode is a thin plate. It is filled with $\mathrm{Ar/CO_2}$ (80%/20%) as detection medium. A second filter made of iron (brown) follows the tracking system. It filters out any muons with

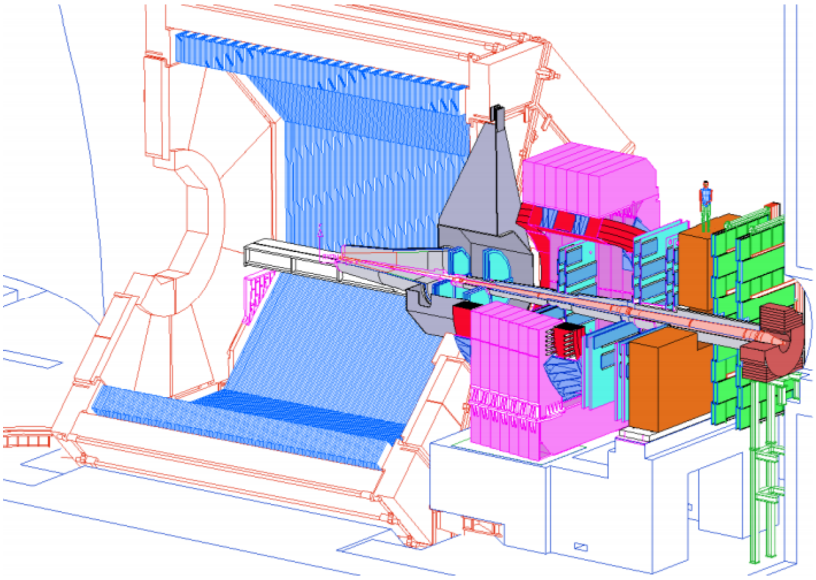

Figure 3.3: Schematic view of the ALICE Muon Spectrometer. Taken from [Aam+08, p. 106, Fig. 4.1].

a momentum smaller than 4 GeV and decelerates the remaining muons to protect the following trigger system from high energy particles. The trigger system consists of two layers of Resistive Plate Chambers (RPC) (green). Those provide time information of the particles to be detected. All in all, the Muon Spectrometer can detect muons including their momentum and electric charge sign. This enables J/ψ detection via the J/$\psi \to \mu^+\mu^-$ decay channel [Aam+08].

3.2 ATLAS and LHCb

Besides ALICE, the ATLAS and LHCb collaboration also published datasets of J/ψ cross sections. ATLAS is a multi-purpose detector. The ATLAS Muon Spectrometer has a pseudorapidity acceptance of $|\eta| \leq 2.4$ [Aab+18]. It detects J/ψ mesons using the dimuon decay channel.

The LHCb detector is specifically designed for the detection of charm and bottom quarks. It has a pseudorapidity acceptance of $2 \leq \eta \leq 5$ for J/ψ detection in the dimuon decay channel [Aai+15].

3.3 Datasets

There are several different datasets of various collaboration which provide J/ψ and ψ(2S) cross sections for $\sqrt{s} = 5.02$ TeV and $\sqrt{s} = 13$ TeV in pp collisions. At $\sqrt{s} = 5.02$ TeV

ALICE published data for J/ψ generation recorded in a 2017 pp run [Ach+19]. The ATLAS collaboration published data with J/ψ cross sections at the same energy. The data include a differentiation between prompt and $B \to$ J/ψ (non-prompt) J/ψ-particles [Aab+18]. The data originate from a 2015 pp run. For $\sqrt{s} = 13\,\mathrm{TeV}$ there is a dataset from ALICE with data of an 2015 pp run [Ach+17]. The dataset provides inclusive J/ψ and ψ(2S) cross sections. The LHCb collaboration published a dataset of J/ψ cross section from a 2015 pp run [Aai+15]. The data are differentiated between prompt and non-prompt J/ψ. Finally, there are rapidity distributions $\mathrm{d}\sigma/\mathrm{d}y$ at $\sqrt{s} = 13\,\mathrm{TeV}$ for J/ψ and ψ(2S) by ALICE [Ach+17] and for J/ψ by LHCb [Aai+15].

4 Monte Carlo Simulation

PYTHIA is a program for Monte Carlo event generation in high-energy physics [Sjö+15]. It implements a complex physics model which combines several different processes. In total, pp, $p\bar{p}$, e^-e^- and e^+e^- collisions are available. This enables PYTHIA to generate one kind of events that occur at LHC, which are pp collisions. Every event generated with PYTHIA contains a list of all single particles which were created and eventually decayed after the initial collision of the two protons. The physical quantities of any particle are accessible. Usually many million events are generated to gain enough statistics. This makes it possible to analyse the charmonium production, calculate the cross sections of the charmonia and compare them to experimental data collected by ALICE and the other LHC experiments. Afterwards it is possible to evaluate the quality of PYTHIA's charmonium simulation capabilities. In a further step one can tune the physics models implemented in PYTHIA to improve the charmonium simulation processes. Additionally to charmonium production, a basic analysis in bottomonium production will be done in order to understand non-prompt charmonium production.

4.1 PYTHIA Setup

The physics implementation in PYTHIA offers prebuilt *tunes* with a variety of different parameter sets. One frequently used tune is the *Monash 2013 Tune* [SCR14]. It provides up-to-date adjustment of the PYTHIA parameters to the current state of physics research. This tune was created with experimental data of LEP, SLD, SPS, Tevatron and LHC experiments. The largest centre-of-mass energy appearing in the data is $\sqrt{s} = 8\,\text{TeV}$. This is only about 62% of the currently achievable $\sqrt{s} = 13\,\text{TeV}$. The tune is available via the PYTHIA setting Tune:pp = 14 and will be used in all following simulations. All calculations are done using the version PYTHIA 8.240. The settings Beams:idA and Beams:idB define the particles to be collided. They are set to 2212 which is the PDG code for a proton according to the *Monte Carlo Particle Numbering Scheme* published in "Review of Particle Physics" [Tan+18]. The setting Beams:eCM defines the centre-of-mass energy $\sqrt{s}$ of the collision partners given in GeV. Finally, SoftQCD:inelastic = on is set. This enables minimum bias event generation and the maximum number of particles to be taken into account for correct cross section calculation. For every centre-of-mass energy $\sqrt{s}$, 500 million events are generated.

4.2 Comparability of Simulation Results

The physical quantity given by most of the experiments is the double-differential cross section $\frac{\mathrm{d}^2\sigma}{\mathrm{d}p_\mathrm{T}\mathrm{d}y}$. It is a measure for the probability of a certain process in a given transverse momentum Δp_T and rapidity Δy range to happen. PYTHIA calculates an estimated cross section σ_gen for any implemented and activated process that can occur in the simulation. The final cross section for a specific process can be calculated using

$$\frac{\mathrm{d}^2\sigma_\mathrm{process}}{\mathrm{d}p_\mathrm{T}\mathrm{d}y} = \sigma_\mathrm{gen} \cdot \frac{N_\mathrm{obsv}}{N_\mathrm{events}} \cdot \frac{1}{\Delta p_\mathrm{T} \cdot \Delta y} \tag{4.1}$$

where N_obsv is the number of times this process was observed in all events of the simulation and N_events is the total number of events generated. The division by Δp_T and Δy is necessary to properly normalise the cross section by the bin widths used. Ideally, the total acceptance ranges for both transverse momentum p_T and rapidity y match the ones of the ALICE experiment. Most datasets were recorded using the dimuon decay channel and the Muon Spectrometer which has a pseudorapidity acceptance of $-4 \leq \eta \leq -2.5$. Due to the symmetry of proton-proton collisions the signs of the pseudorapidity and rapidity can be neglected. Therefore, particles with $2.5 \leq |y| \leq 4$ are taken into account in the simulation. However, the rapidity bin size Δy doubles from 1.5 to 3 in this case. The other datasets detect electron pairs using the ITS and TPC of ALICE with a rapidity of $|\eta| \leq 0.9$. The rapidity acceptance range is set to $|y| \leq 0.9$ in the simulation with $\Delta y = 1.8$ accordingly. $\Delta p_\mathrm{T} = 1\,\mathrm{GeV}$ is set as transverse momentum bin size if not noted otherwise. For relative plots as "experimental data / PYTHIA", the internal PYTHIA bins are rebinnend to the size of the experimental data bins.

At $\sqrt{s} = 13\,\mathrm{TeV}$ a comparison of the rapidity distributions to existing ALICE datasets is possible, due to availability of those measurements. The J/ψ simulation is cut at $p_\mathrm{T} \leq 30\,\mathrm{GeV}$ in accordance with the ALICE data. The LHCb data offer a cut with $p_\mathrm{T} < 14\,\mathrm{GeV}$. The impact of this difference will be discussed in the analysis chapter. At $\sqrt{s} = 5.02\,\mathrm{TeV}$, no such comparison is possible, as those datasets are not published yet. The $\psi(2\mathrm{S})$ in the simulation are cut with $p_\mathrm{T} \leq 16\,\mathrm{GeV}$ according to the corresponding ALICE data. A rapidity bin size of $\Delta y = 0.5$ is set.

4.3 $b\bar{b}$-Pair Production

To analyse the $b\bar{b}$-pair production, any bare b quark and $\bar{b}$ antiquark within the rapidity range of $2.5 \leq y \leq 4$ are taken into account. This is set in the settings of PYTHIA as well as in the online FONLL form. b quarks are always produced in pairs of b and $\bar{b}$. Therefore, the PYTHIA code looks for pairs of b and $\bar{b}$. Such a pair is found if a particle has two daughters of which one is b and the other $\bar{b}$. The transverse momentum of the $b\bar{b}$-pair is the vector sum of the b and the $\bar{b}$ momenta. The resulting cross section spectrum can then be compared to the FONLL calculations.

5 Data Analysis

The comparison of the different cross sections is done separately for different the centre-of-mass energies $\sqrt{s}$. First, PYTHIA-simulated J/ψ cross sections at $\sqrt{s} = 5.02\,\mathrm{TeV}$ are compared to measurements. Afterwards, simulated cross sections of J/ψ and ψ(2S) at $\sqrt{s} = 13\,\mathrm{TeV}$ are compared to measurements. Finally, a comparison of PYTHIA-simulated bottom production cross sections to FONLL calculations is given.

The datasets differentiate between statistical uncertainties σ_{stat} and systematic uncertainties σ_{syst}. In the absolute cross section plots, the uncertainties are drawn separately just as in the respective original publications. The uncertainties are added up in quadrature in order to get a single uncertainty value σ_{exp} for the experimental results in relative plots:

$$\sigma_{\mathrm{exp}} = \sqrt{\sigma_{\mathrm{stat}}^2 + \sigma_{\mathrm{syst}}^2}. \tag{5.1}$$

In case the integrated luminosity uncertainty σ_{lumi} and the branching ratio uncertainty σ_{BR} are given separately, they are also taken into account for a total uncertainty in relative plots according to

$$\sigma_{\mathrm{exp}} = \sqrt{\sigma_{\mathrm{stat}}^2 + \sigma_{\mathrm{syst}}^2 + \sigma_{\mathrm{lumi}}^2 + \sigma_{\mathrm{BR}}^2} \tag{5.2}$$

Let v_{exp} be the experimental result of a measurement and v_{pyt} the result of the same measurement based on a PYTHIA simulation. The associated uncertainties are σ_{exp} and σ_{pyt}. Then the ratio r is calculated by

$$r = \frac{v_{\mathrm{exp}}}{v_{\mathrm{pyt}}} \tag{5.3}$$

with the uncertainty

$$\sigma_{\mathrm{r}} = \sqrt{\left(\frac{1}{v_{\mathrm{pyt}}} \cdot \sigma_{\mathrm{exp}}\right)^2 + \left(-\frac{v_{\mathrm{exp}}}{v_{\mathrm{pyt}}^2} \cdot \sigma_{\mathrm{pyt}}\right)^2} \tag{5.4}$$

according to error propagation for uncorrelated uncertainties.

Note that the approximation $\eta \approx y$ (equation (2.5)) is used all over this chapter. All simulated results use the rapidity y while all experimental results use the pseudorapidity η. The plots only show the rapidity y for reasons of clarity.

5.1 Cross Sections of J/ψ Mesons at $\sqrt{s} = 5.02\,\mathrm{TeV}$

Figure 5.1 shows the differential cross section for inclusive J/ψ at $\sqrt{s} = 5.02\,\mathrm{TeV}$. The PYTHIA simulation results are compared to results from ALICE in the lower p_{T} region and to results from ATLAS in the higher p_{T} region. To PYTHIA and ALICE data a rapidity cut at $|y| \leq 0.9$ and $|\eta| \leq 0.9$ is applied respectively, while the ATLAS data are cut at $|y| \leq 0.75$. For comparability, a separate PYTHIA dataset with $|\eta| \leq 0.75$ is shown in blue with open datapoints. It can be seen, that the cross sections do not differ much between $y \leq 0.75$ and $y \leq 0.9$ in the simulation. The cross sections should still be comparable, because they are normalised with respect to rapidity/pseudorapidity. For $\sqrt{s} = 13\,\mathrm{TeV}$ it is shown in section 5.2, that a change of rapidity does not produce large changes of the cross sections in low rapidity ranges. Due to the lack of y-dependent experimental cross sections at $\sqrt{s} = 5.02\,\mathrm{TeV}$, this can only be presumed for this energy.

The overall trend of the cross sections is predicted well by PYTHIA. There is a cross section maximum at $2 - 3\,\mathrm{GeV}$. This maximum is shifted about $1\,\mathrm{GeV}$ towards lower transverse momenta p_{T} in the experimental data. The curve is decreasing monotonously on both sides of the maximum. In figure 5.2 a ratio of the experimental cross sections to the PYTHIA cross sections can be seen. In the lowest p_{T} bin, the measured production of J/ψ particles is about 1.8 times higher than PYTHIA predicts. This overestimation decreases with increasing transverse momentum. At around $3\,\mathrm{GeV}$ the experimental cross section is predicted correctly by PYTHIA. With further increasing p_{T}, PYTHIA begins to overestimate the J/ψ production up to a factor of about 2. The curve does not decrease fully monotonously, but the uncertainty intervals overlap in a way, that a monotonous curve is possible.

There are separate datasets for prompt and non-prompt J/ψ at $\sqrt{s} = 5.02\,\mathrm{TeV}$. Figure 5.3 shows the cross sections for prompt J/ψ compared to ATLAS data. In figure 5.4 one can see a ATLAS / PYTHIA ratio plot. The ATLAS dataset starts at $p_{\mathrm{T}} = 8\,\mathrm{GeV}$. At higher p_{T} than the maximum, the cross sections of J/ψ decrease with increasing transverse momentum in the PYTHIA data as well as in the ATLAS data. The ratio reveals that the production of prompt J/ψ is overestimated by up to a factor of 2. The factor is more or less constant over changing transverse momenta. Figure 5.5 and figure 5.6 show the same plots for $B \to \mathrm{J}/\psi$ (non-prompt) J/ψ particles. Again, PYTHIA and ATLAS data show a decreasing cross section for increasing transverse momenta higher than the cross section maximum. The production is overestimated by a factor of 2 again (see figure 5.6). The ratio varies between around 0.4 and 0.8, but the uncertainties all include a common ratio of about $0.5 - 0.6$.

At $\sqrt{s} = 5.02\,\mathrm{TeV}$ PYTHIA underestimates the J/ψ production in lower p_T regions and overestimates it in higher p_T regions. The latter can also be observed for prompt and non-prompt J/ψ production independently in higher p_T regions. The PYTHIA prediction agrees with the experimental results at about $p_\mathrm{T} \approx 3\,\mathrm{GeV}$.

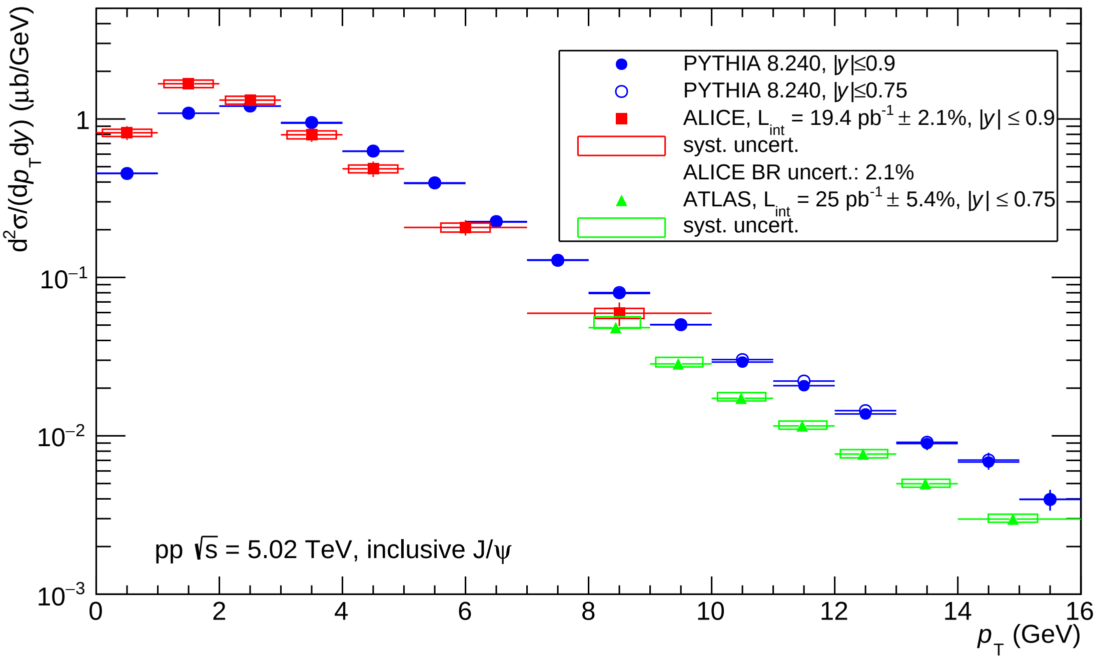

Figure 5.1: Inclusive p_T-differential J/ψ cross section at $\sqrt{s} = 5.02\,\mathrm{TeV}$. The cross sections calculated using PYTHIA are shown in blue. The cross sections are compared to experimental results of ALICE and ATLAS at the same $\sqrt{s}$. Note that the ATLAS rapidity range does not exactly match the rapidity range of ALICE data. Therefore, the open blue datapoints show PYTHIA cross sections with an ATLAS rapidity cut.

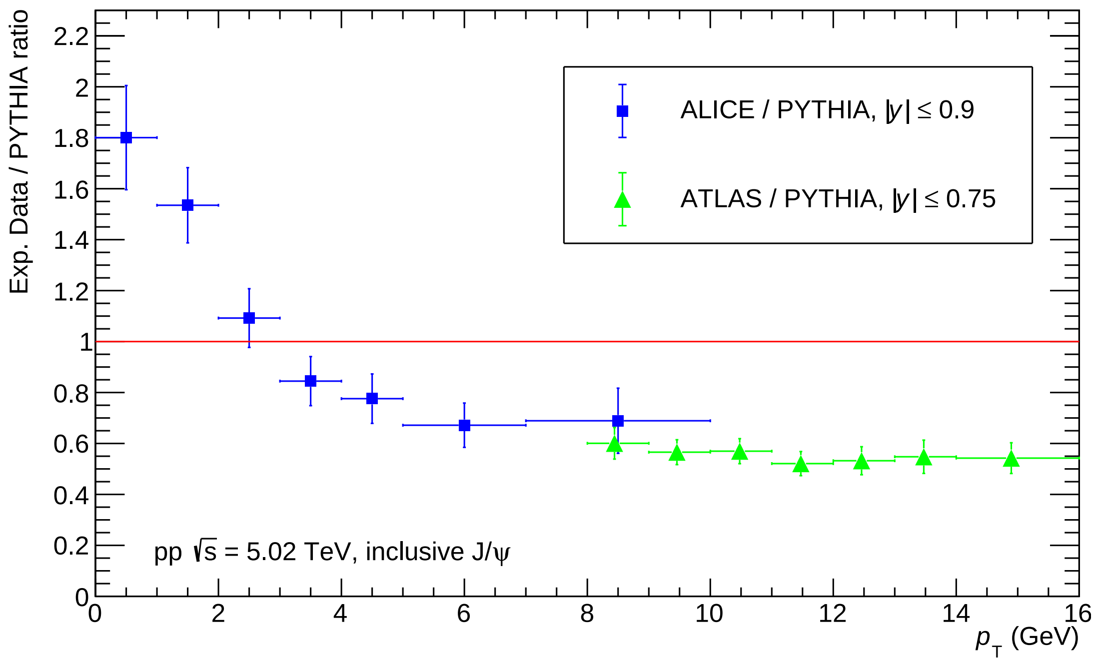

Figure 5.2: Ratio of experimental p_T-differential inclusive cross sections and simulated inclusive cross sections for J/ψ at $\sqrt{s} = 5.02\,\mathrm{TeV}$. The experimental data originate from the ALICE and ATLAS experiments.

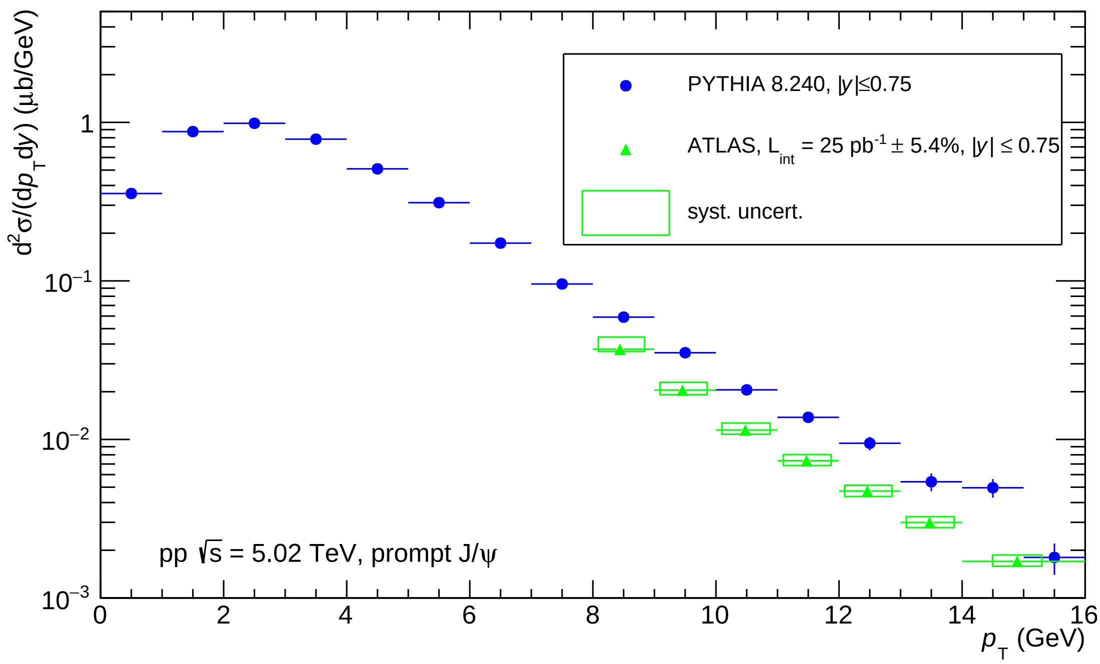

Figure 5.3: p_T-differential cross section for prompt J/ψ at $\sqrt{s} = 5.02\,\mathrm{TeV}$. The cross sections calculated using PYTHIA are shown in blue. The cross sections are compared to experimental results of ATLAS at the same $\sqrt{s}$.

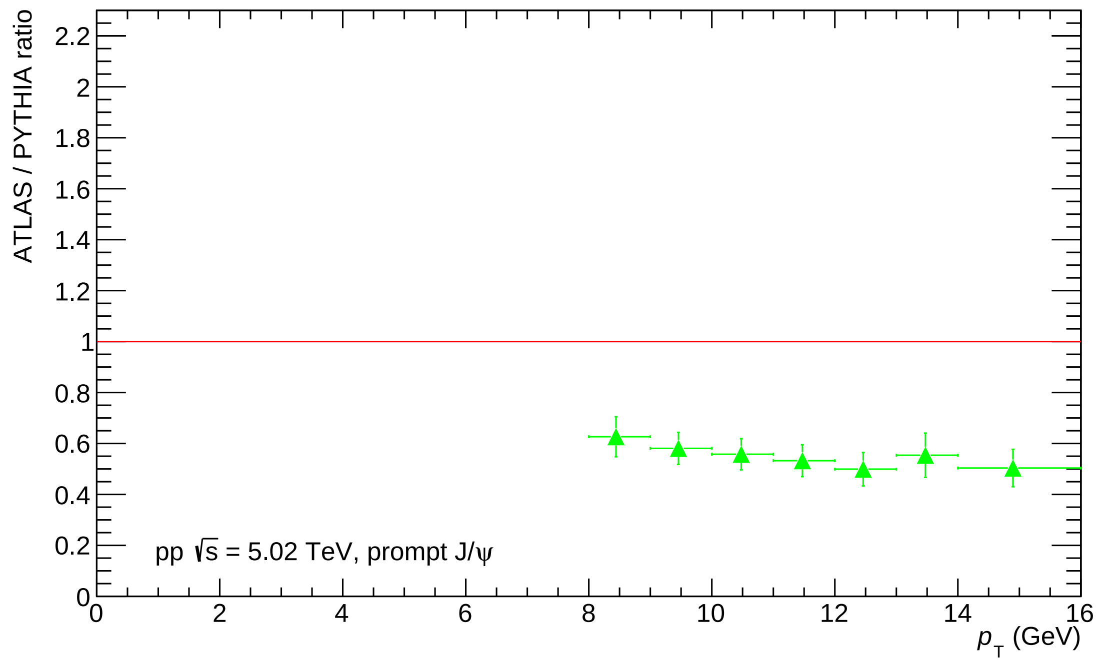

Figure 5.4: Ratio of ATLAS and PYTHIA p_T-differential cross sections for prompt J/ψ at $\sqrt{s} = 5.02\,\mathrm{TeV}$. The rapidity is cut at $|y| \leq 0.75$ in both datasets.

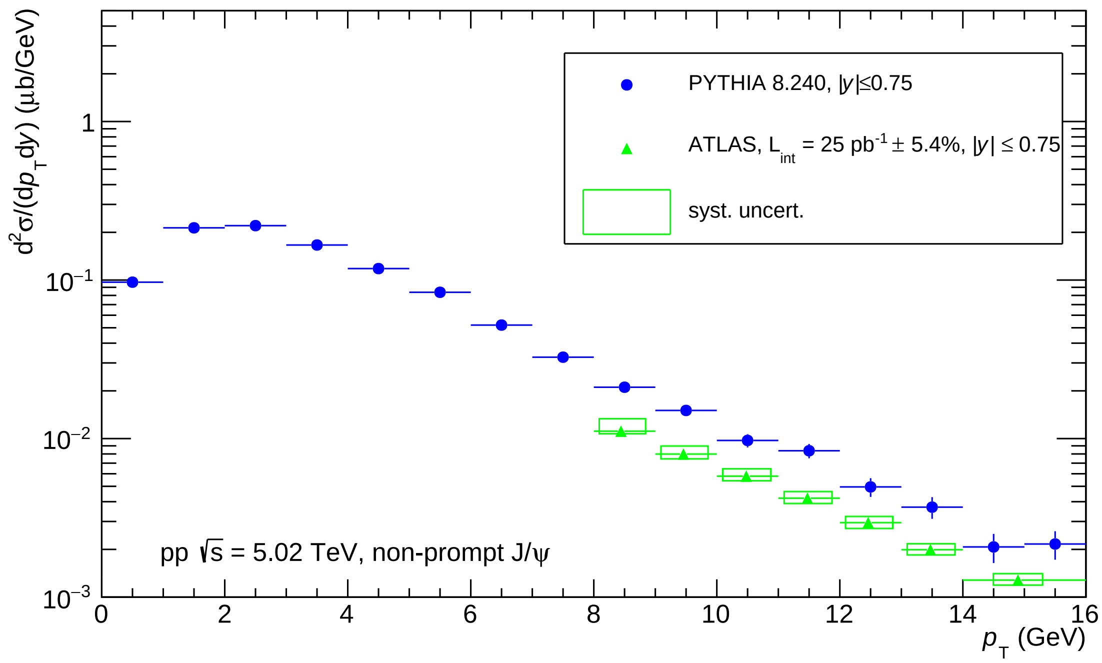

Figure 5.5: p_T-differential cross section for non-prompt J/ψ at $\sqrt{s} = 5.02\,\mathrm{TeV}$. The cross sections calculated using PYTHIA are shown in blue. The cross sections are compared to experimental results of ATLAS at same $\sqrt{s}$.

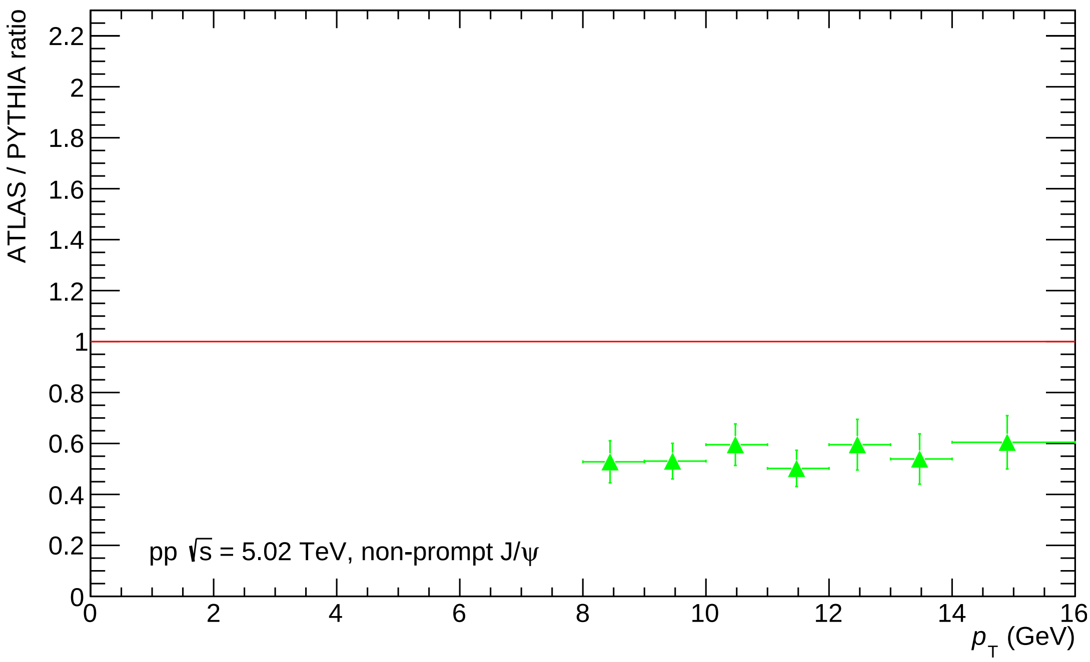

Figure 5.6: Ratio of ATLAS and PYTHIA p_{T}-differential cross sections for non-prompt J/ψ at $\sqrt{s} = 5.02\,\mathrm{TeV}$. The rapidity is cut at $|y| \leq 0.75$ in both datasets.

5.2 Cross Sections of J/ψ Mesons at $\sqrt{s} = 13\,\mathrm{TeV}$

In figure 5.7, J/ψ cross sections calculated using PYTHIA simulations at $\sqrt{s} = 13\,\mathrm{TeV}$ are compared to ALICE and LHCb data. Figure 5.8 shows a ratio plot of the cross sections. All datasets show a maximum of the cross section. It lies at $1-2\,\mathrm{GeV}$ for the two experimental datasets. The PYTHIA maximum lies at $2-3\,\mathrm{GeV}$ and slightly smaller than the maximum of the experimental data cross sections. All cross section curves provide a monotonous decrease on both sides of the maximum. In the lowest p_{T} bin $(0-1\,\mathrm{GeV})$ the ratio reaches its highest value of about 2.1. In this p_{T} range the production of inclusive J/ψ is heavily underestimated by PYTHIA. This changes with increasing transverse momentum. The prediction is in agreement with the results from the experiments for $p_{\mathrm{T}} \approx 3\,\mathrm{GeV}$. With further increasing p_{T} PYTHIA starts to overestimate the J/ψ production up to a factor of 0.4. This result is consistent with the behaviour of the J/ψ cross section at $\sqrt{s} = 5.02\,\mathrm{TeV}$. There exist prompt and non-prompt datasets from LHCb. Those data are compared to PYTHIA data in figure 5.9 and figure 5.10 for prompt J/ψ and figure 5.11 and figure 5.12 for non-prompt J/ψ. The prompt J/ψ production shows the same shift of the cross section maximum to higher p_{T} as observed in the inclusive spectrum. At $p_{\mathrm{T}} < 3\,\mathrm{GeV}$ the prompt J/ψ production is underestimated while at $p_{\mathrm{T}} > 3\,\mathrm{GeV}$ production cross is overestimated. At close-to-zero transverse momenta, the factor is as high as 2.3 and it goes down for higher p_{T} to about 0.5.

The trend at higher p_T is consistent with the results at $\sqrt{s} = 5.02\,\text{TeV}$. There are no prompt J/$\psi$ data published at lower p_T and $\sqrt{s} = 5.02\,\text{TeV}$.

The non-prompt data do not show a shift of the maximum. The maximum is reached at around 2 GeV for PYTHIA and LHCb data. Interestingly, the prediction of non-prompt J/ψ production is not underestimated at small p_T. Instead the production is overestimated by a factor of about 0.4 – 0.6 over the whole transverse momentum spectrum. Due to the uncertainties, a constant factor is possible. To further investigate this process, the $b\bar{b}$ production is analysed in section 5.4.

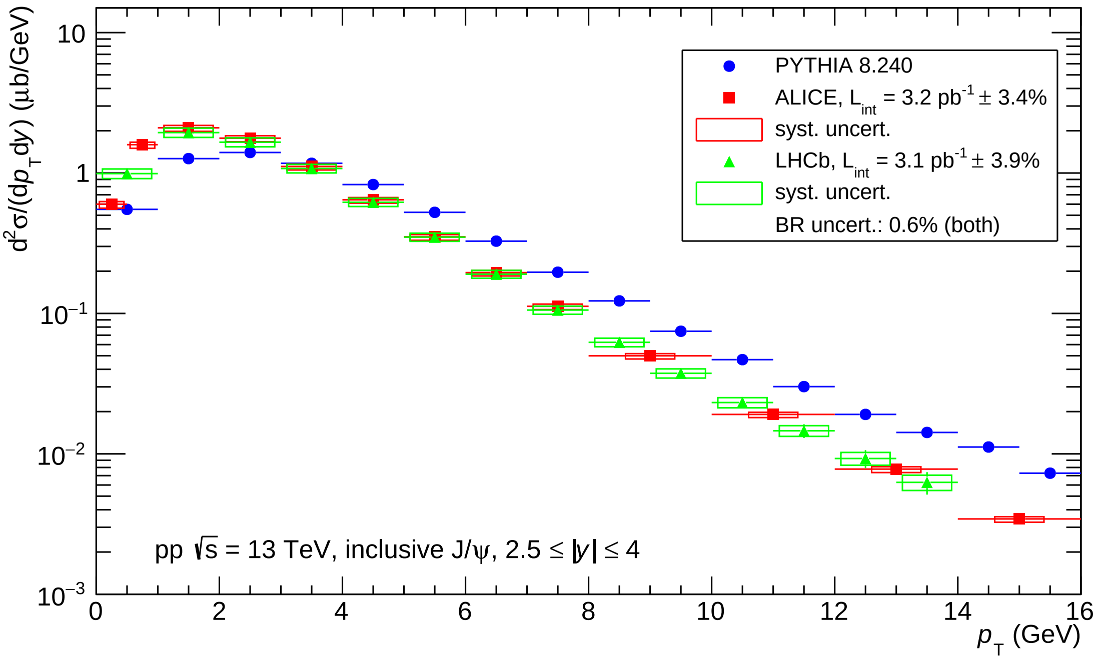

Figure 5.7: Inclusive p_T-differential J/ψ cross section at $\sqrt{s} = 13\,\text{TeV}$. The cross sections calculated using PYTHIA are shown in blue. The cross sections are compared to experimental results of the ALICE and LHCb at same $\sqrt{s}$ and rapidity range.

In figure 5.13 a comparison of y-differential cross sections is done. There are filled blue datapoints for a 30 GeV p_T cut in the PYTHIA cross sections and open datapoints for a 14 GeV p_T cut. The first one corresponds to the ALICE measurement and the latter one to the LHCb measurement. The cross sections with the lower p_T cut do not differ significantly from the cross sections with the higher cut, as not many J/ψ with a high transverse momentum get produced. The experimental data from ALICE and LHCb span a rapidity range from 2.5 – 4 and 2 – 4.5 respectively. At a higher rapidity of about 3.5 – 4.5 the experimental results agree with the PYTHIA-simulated cross sections. The cross section is about 5 µb at $y = 4$. The cross sections increase with decreasing magnitude of rapidity. The ALICE cross sections have a higher gradient than the LHCb and PYTHIA ones. The LHCb measurement

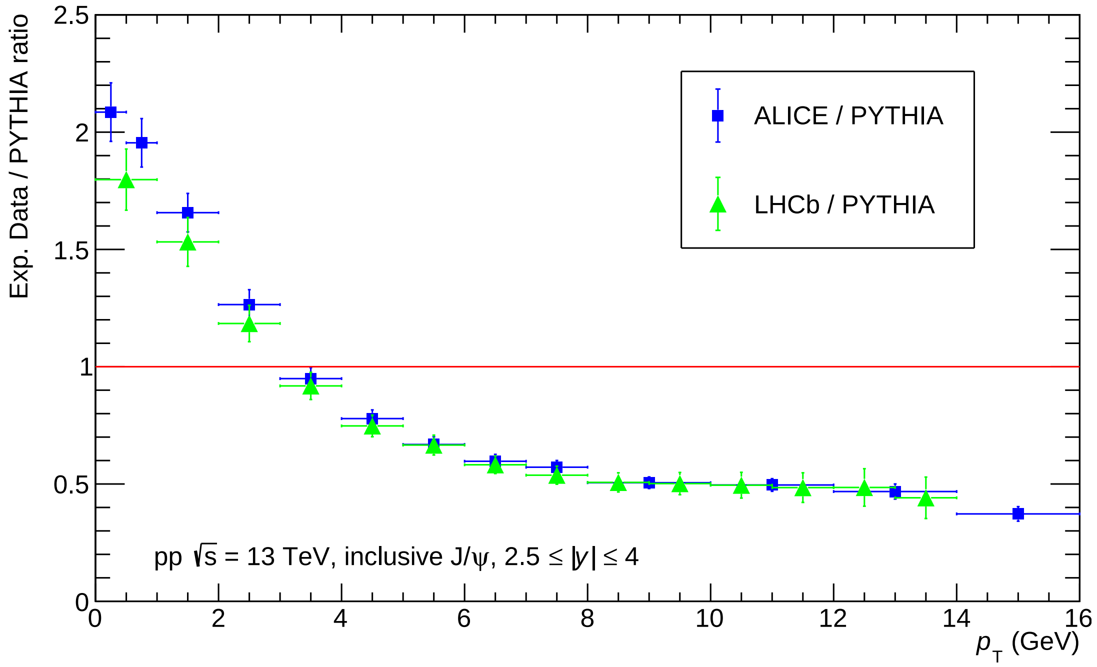

Figure 5.8: Ratio of experimental p_T-differential inclusive cross sections and simulated inclusive cross sections for J/ψ at $\sqrt{s} = 13\,\mathrm{TeV}$. The experimental data originate from the ALICE and LHCb experiments.

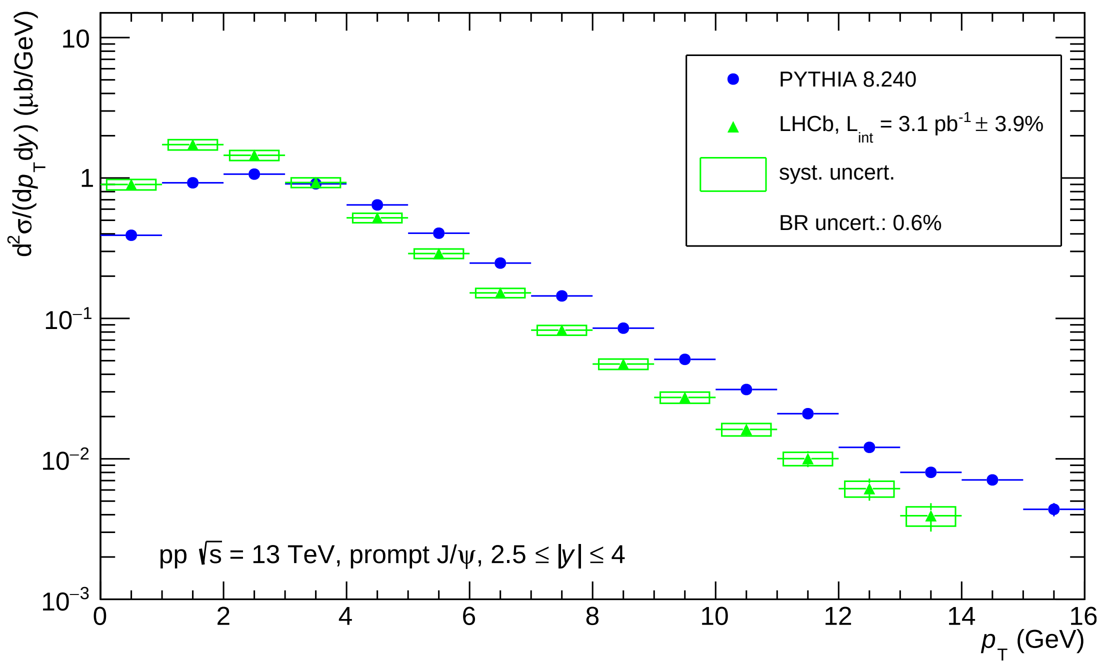

Figure 5.9: p_T-differential cross sections for prompt J/ψ at $\sqrt{s} = 13\,\mathrm{TeV}$. The PYTHIA results are compared to the LHCb results at same $\sqrt{s}$ and rapidity.

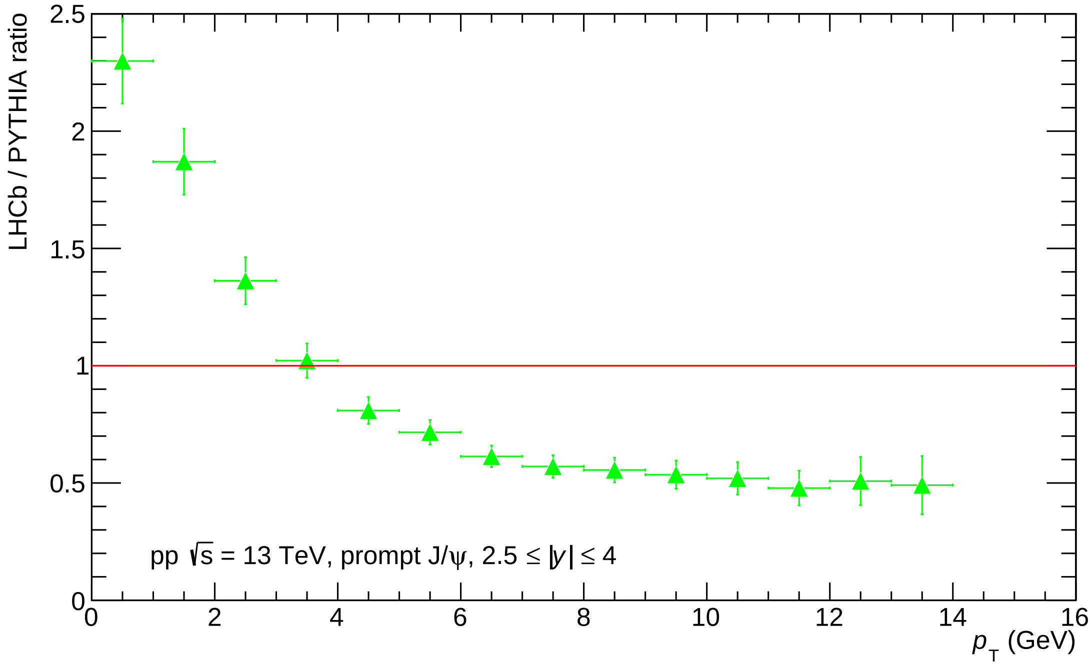

Figure 5.10: Ratio of LHCb and PYTHIA p_{T}-differential cross sections for prompt J/ψ at $\sqrt{s} = 13\,\mathrm{TeV}$.

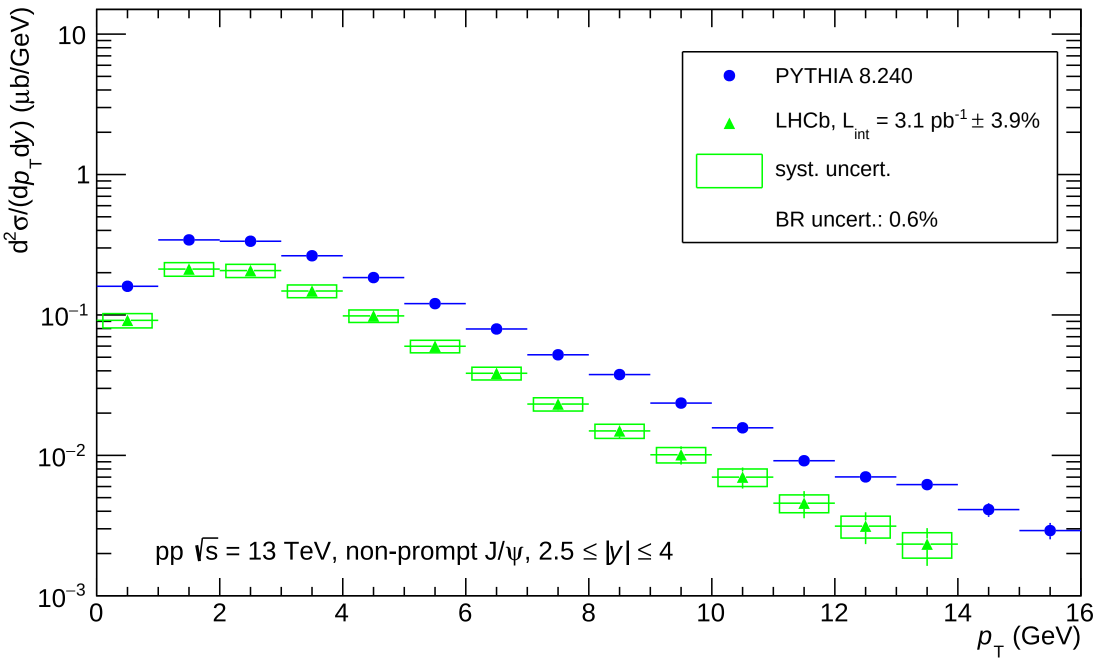

Figure 5.11: p_{T}-differential cross sections for non-prompt J/ψ at $\sqrt{s} = 13\,\mathrm{TeV}$. The PYTHIA results are compared to the LHCb results at same $\sqrt{s}$ and rapidity.

seems to fit the trend of the PYTHIA cross sections better. For the first and the last rapidity bin within the LHCb rapidity range, the PYTHIA cross sections fall into the 1σ-interval of

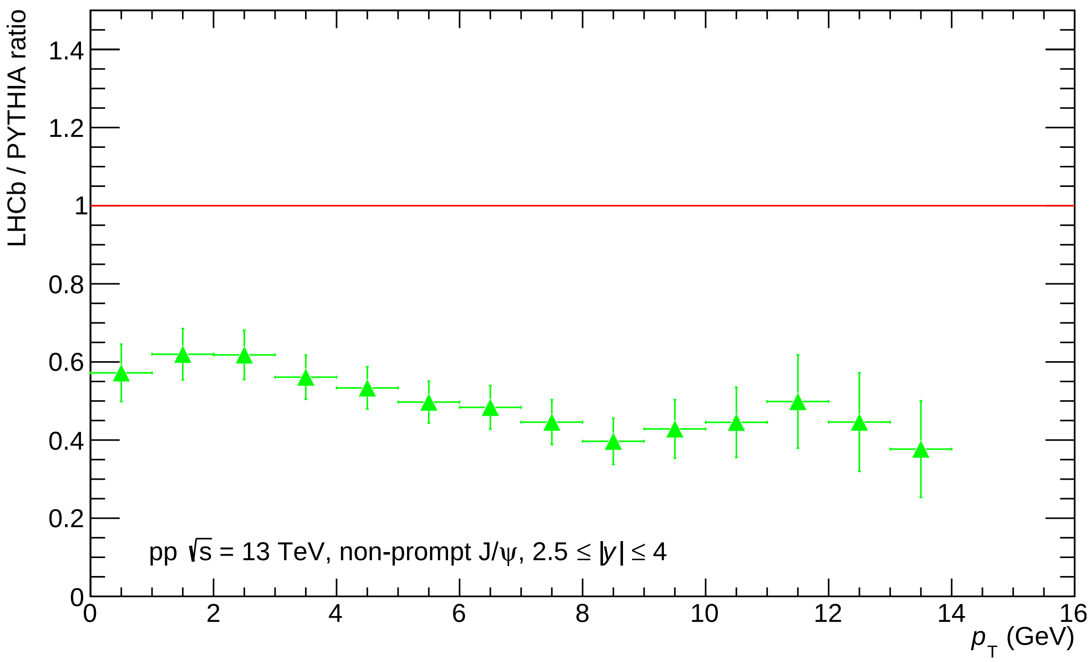

Figure 5.12: Ratio of LHCb and PYTHIA p_T-differential cross sections for non-prompt J/ψ at $\sqrt{s} = 13\,\mathrm{TeV}$.

the LHCb uncertainties. For the remaining three bins the PYTHIA cross sections fall in the 2σ-interval. This can also be seen in figure A.1 in the appendix, which provides a zoomed view of the plot given here. The LHCb data were cut at $p_\mathrm{T} < 14\,\mathrm{GeV}$ while the ALICE data go up to $30\,\mathrm{GeV}$. The open datapoints show PYTHIA cross sections with the same $p_\mathrm{T} < 14\,\mathrm{GeV}$ cut as LHCb. The adjustment of the p_T cut does not change the cross sections significantly.

Going from the $4-4.5$ rapidity bin to the $2-2.5$ bin results approximately in a doubling of the cross section. This can be observed in the simulation as well as in the LHCb measurements. The difference between the $2-2.5$ and $0-0.5$ rapidity bin in the PYTHIA data is much lower. In this range the cross section increases from about $8\,\mu\mathrm{b}$ to about $9.5\,\mu\mathrm{b}$. A pseudorapidity cut change from $|\eta| \leq 0.9$ to $|\eta| \leq 0.75$ presumably will not change the double-differential cross sections significantly, because the p_T integrated cross sections in figure 5.13 do not differ much from each other. This can also be seen in figure A.2 in the appendix. In that plot, no rebinning to larger bins is done. In section 5.1, ALICE data with an pseudorapidity cut of $|\eta| \leq 0.9$ were compared to ATLAS data with a $|\eta| \leq 0.75$ cut at $\sqrt{s} = 5.02\,\mathrm{TeV}$. This is still reasonable under the presumption, that the cross sections behave similar at the lower energy.

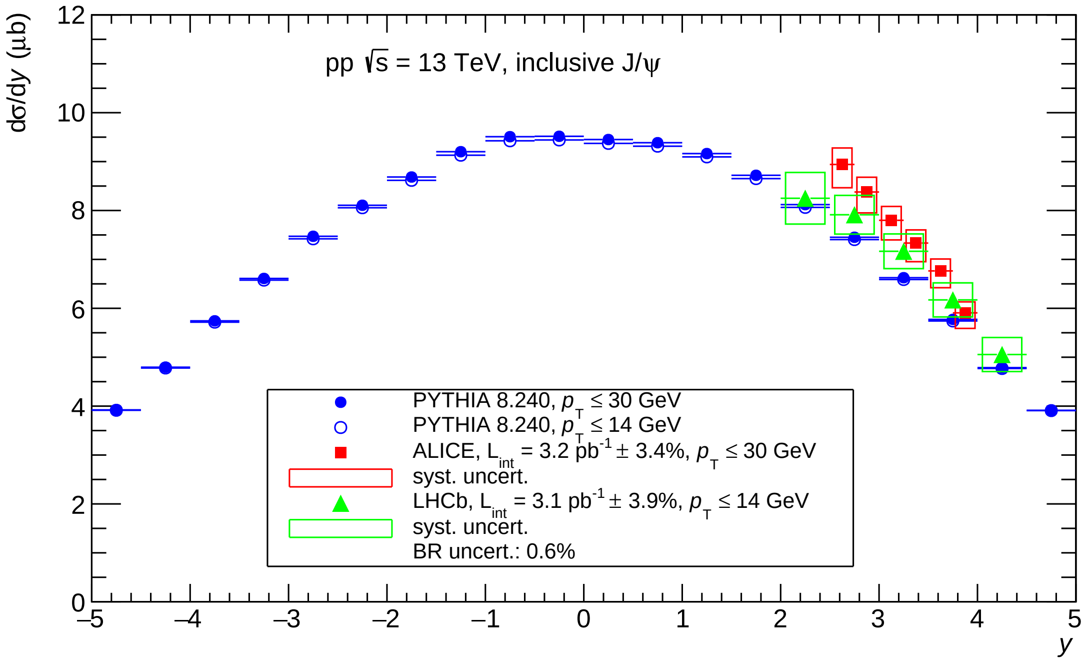

Figure 5.13: y-differential inclusive J/ψ cross section at $\sqrt{s} = 13\,\mathrm{TeV}$. The results are compared to ALICE and LHCb data.

5.3 Cross Sections of $\psi(2\mathrm{S})$ Mesons at $\sqrt{s} = 13\,\mathrm{TeV}$

The ALICE collaboration has published differential cross sections for $\psi(2\mathrm{S})$ at $\sqrt{s} = 13\,\mathrm{TeV}$. These were also calculated by PYTHIA. The resulting cross sections can be seen in figure 5.14 and figure 5.15. The trend of the PYTHIA cross sections is in agreement with the measurement. There is a maximum of the cross section at $1-2\,\mathrm{GeV}$. For higher p_{T}, the cross sections decrease with increasing p_{T}, although the curves fluctuate more than in J/ψ cross section measurements or simulations. Additionally, the systematical and statistical uncertainties of the ALICE measurement and the statistical uncertainties of PYTHIA simulations are larger than the respective uncertainties observed in J/ψ cross section measurements and simulations. The absolute cross sections differ very much between measurement and simulation. The cross section is up to 12 times higher than predicted by PYTHIA simulations. This underestimation is reduced to about 4 for the higher p_{T} bins. However, the prediction of $\psi(2\mathrm{S})$ generation in PYTHIA clearly deviates much more from experimental results as the prediction of J/ψ generation does. Additionally, the uncertainties of the datasets are relatively small compared to the absolute deviation of the cross sections. The statistical uncertainty of the simulation together with the statistical and systematical uncertainty of the ALICE measurement can not explain this deviation. It is possible, that the underlying PYTHIA physics model just does not describe the real process of $\psi(2\mathrm{S})$ production good enough.

Finally, a rapidity dependent cross section for $\psi(2S)$ is given in figure 5.16. The $\psi(2S)$ cross section has a maximum at zero rapidity. It decreases with increasing magnitude of rapidity. The cross sections do not decrease monotonously, but this does most likely result from statistical deviations as it only concerns two single bins from $y = -1$ to $y = -0.5$ and $y = 2.5$ to $y = 3$. Again, it can be observed that the generation of $\psi(2S)$ mesons is underestimated over the whole rapidity range of the ALICE measurement.

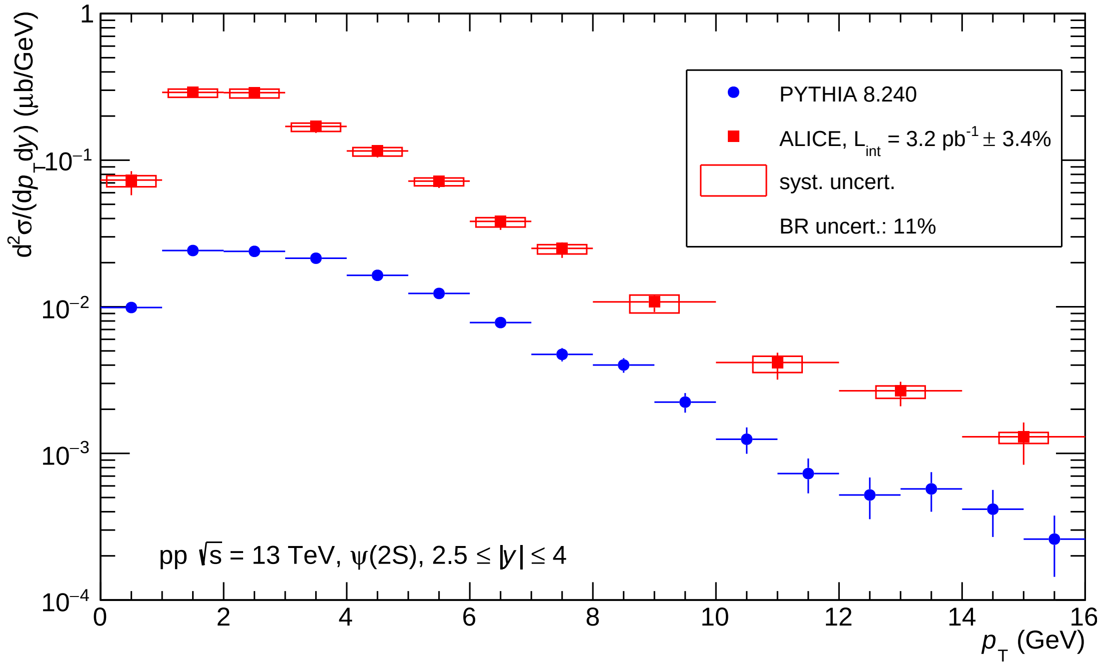

Figure 5.14: Inclusive p_T-differential $\psi(2S)$ cross section at $\sqrt{s} = 13\,\text{TeV}$. The cross sections are compared to ALICE data.

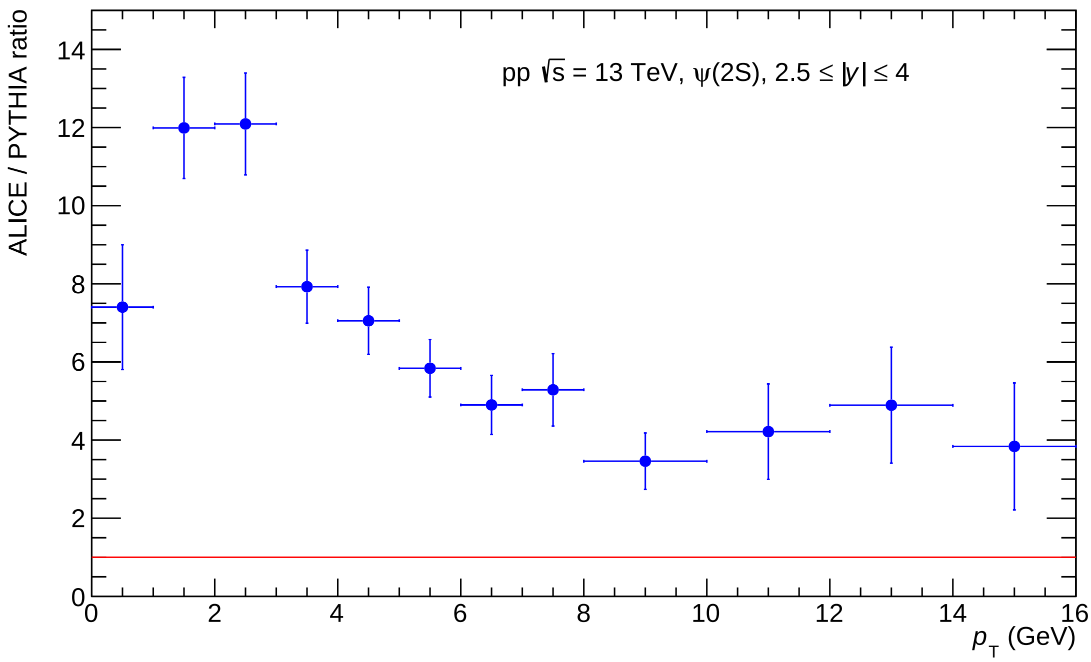

Figure 5.15: ALICE to PYTHIA inclusive $\psi(2S)$ cross section ratio at $\sqrt{s} = 13\,\mathrm{TeV}$.

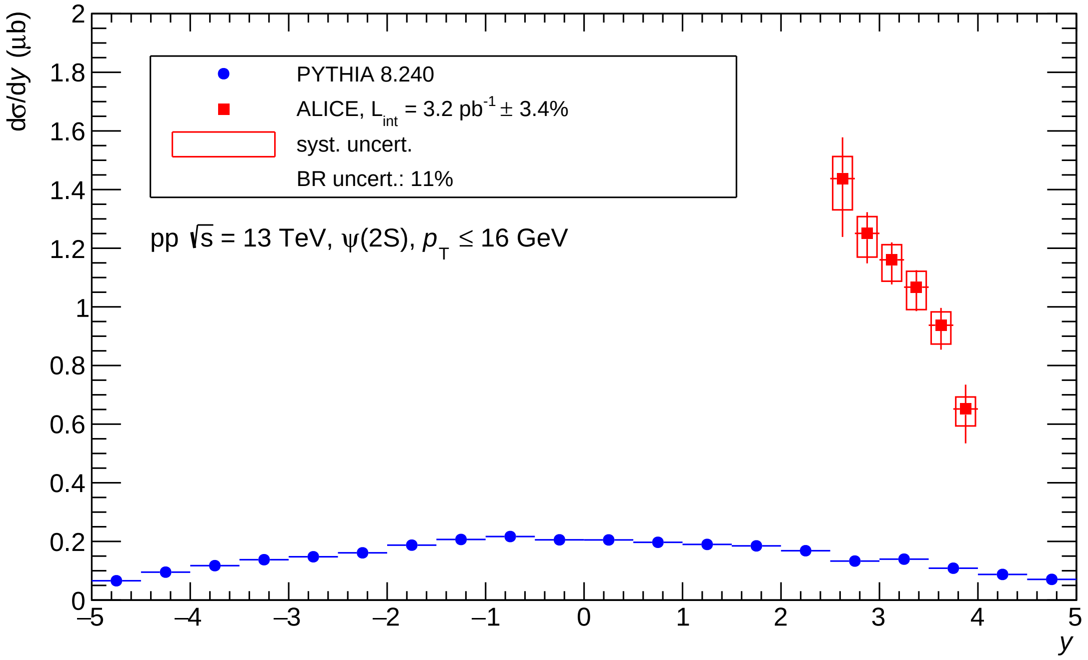

Figure 5.16: y-differential inclusive $\psi(2S)$ cross section compared to ALICE data.

5.4 Comparison of $b\bar{b}$-Pair Production

For a further investigation of the non-prompt J/ψ production, the production of b-quarks is analysed here. Therefore, the b production cross section is determined with PYTHIA. This result can be compared to Fixed-Order Next-to-Leading Logarithm (FONLL) calculations [CGN98; Cac+12]. Those calculations are a theoretical approach to the cross sections of heavy quark (charm and bottom) production. Figure 5.17 shows the $b\bar{b}$-pair cross sections at $\sqrt{s} = 13\,\mathrm{TeV}$. The PYTHIA cross sections only include the statistical uncertainty, while the FONLL results include scale, mass and parton distribution function (PDF) uncertainties. Therefore, the uncertainties of FONLL calculations are much larger. The coloured band in the plot marks the area between the minimum and maximum value of the combined uncertainties. For transverse momenta smaller than around 22 GeV, the PYTHIA-predicted cross sections fall into the FONLL-calculated uncertainty band. For larger transverse momenta, the PYTHIA-predicted cross sections are smaller than the minimum values calculated by FONLL. A step in the PYTHIA cross section spectrum is observable $p_\mathrm{T} \approx 5\,\mathrm{GeV}$. This is most probably not only due to statistical fluctuations, because the statistical uncertainties are rather small over the whole spectrum. However, such a step is not expected in the cross section spectrum. This is unphysical and likely to be a consequence of the PYTHIA physics model. It is highly non-trivial to see what causes this behaviour. Because of this, only a description of the error is given here. In figure 5.18, a ratio plot of the cross sections is shown. The datapoints are the calculated ratios of the cross sections and the light blue area is the uncertainty band. The step at 5 GeV originating from the PYTHIA simulation is also clearly visible in the ratio here. For transverse momenta $< 3\,\mathrm{GeV}$, PYTHIA is likely to slightly overestimate the $b\bar{b}$ production. Behind the previously described step at about 6 GeV the simulation is in agreement with the calculations. For higher p_T, this turns into an underestimation, which changes again into an overestimation at about 14 GeV.

In general the PYTHIA prediction is in agreement with the FONLL calculation for moderate ($p_\mathrm{T} < 22\,\mathrm{GeV}$) transverse momenta. For higher p_T, the cross sections are predicted outside of the FONLL uncertainty band, but the overall shape of the curve is still similar. The main reason for this specific analysis was to understand the source of the deviation in non-prompt J/ψ production. In figure 5.12, the ratio of experimental data to the results from PYTHIA simulation is constant at about $0.4 - 0.6$. This is probably not a direct consequence of the $b\bar{b}$-production. It is no constant overestimation observable here. Instead, the deviation of the simulation to the measurement is p_T-dependent. With that found out, it can be presumed, that the source of the overestimation of non-prompt J/ψ in PYTHIA lies somewhere in the process of the bottom-flavoured particles decaying into charmed particles.

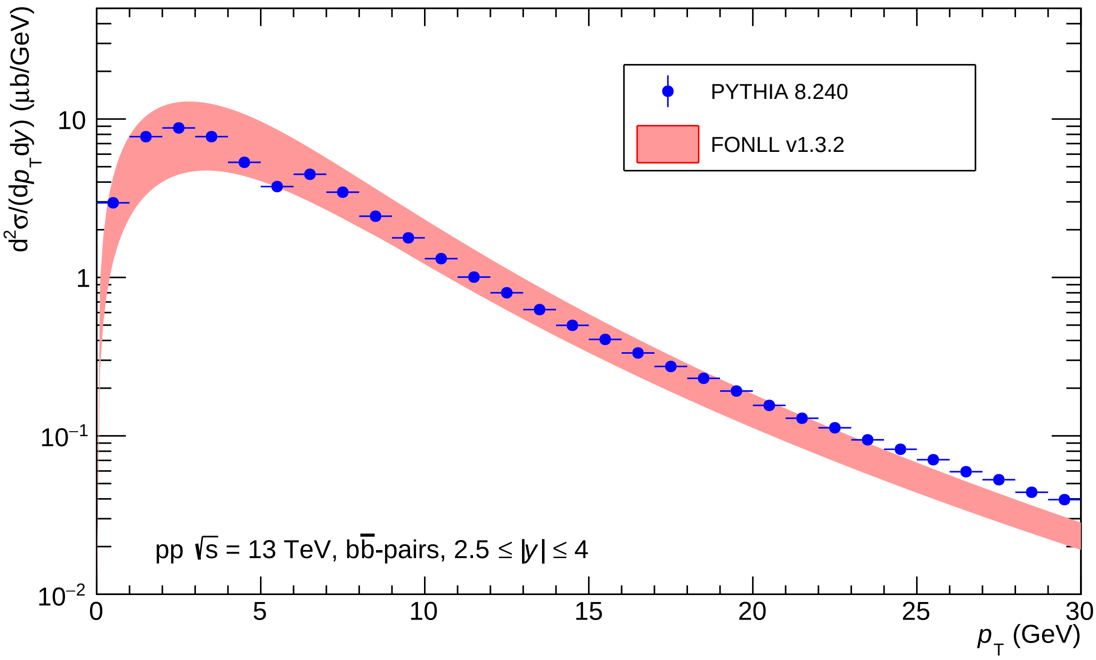

Figure 5.17: p_{T}-differential cross sections of generated $b\bar{b}$-pairs at $\sqrt{s} = 13\,\mathrm{TeV}$. The result is then compared to FONLL calculations.

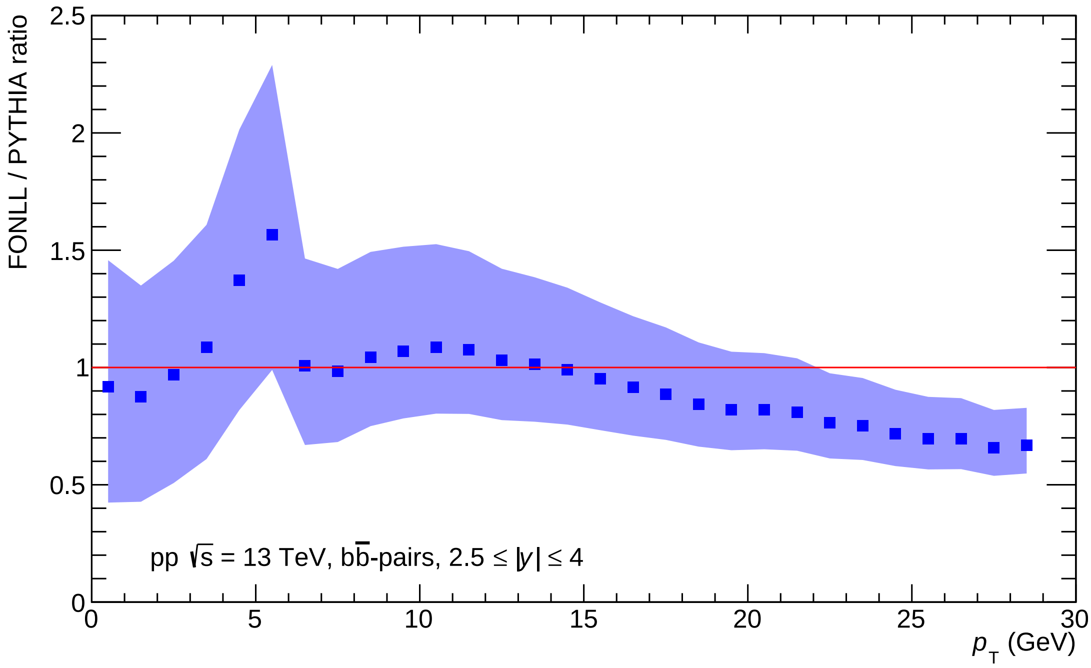

Figure 5.18: FONLL-calculated to PYTHIA-simulated $b\bar{b}$-pair cross section ratio at 13 TeV.

6 Conclusion and Outlook

The production of charmonia, specifically J/ψ and ψ(2S), was simulated with PYTHIA 8.240 and compared to experimental results from the LHC experiments ALICE, ATLAS and LHCb.

Qualitatively, the production of J/ψ particles in PYTHIA is in agreement with measurements. There are clearly visible production maxima in the lower p_{T} range at about 2 GeV in simulated and experimental data. The maxima are shifted about 1 GeV towards higher p_{T} in simulated data compared to measurements. It can be observed, that the inclusive and prompt J/ψ production is underestimated by PYTHIA in p_{T} regions lower than the production maximum and overestimated in higher p_{T} regions. This can be seen at both centre-of-mass energies 5.02 TeV and 13 TeV. The underestimation in lower p_{T} regions seems to be a consequence of the prompt J/ψ production. The non-prompt J/ψ production is overestimated by PYTHIA with a factor of approximately 2 over the whole p_{T} range. In a separate analysis, the production of $b\bar{b}$-pairs was compared to FONLL calculations. There, no such constant factor appears. In fact, a p_{T} dependent under- and overestimation by PYTHIA is observable. Therefore, it is likely, that the process of $b \to$ J/ψ decay is the source of overestimation of non-prompt J/ψ cross section prediction with PYTHIA. Additionally, a prominent and unphysical step in the cross section spectrum is observable at about 5 GeV. Further investigation is needed to fully understand this process in PYTHIA and improve the prediction capabilities.

It has been shown, that the prediction of ψ(2S) production is much more imprecise. There is an underestimation over the whole p_{T} range. The maximum of overestimation is around the production maximum at $p_{\mathrm{T}} \approx 2$ GeV. Going to lower and higher transverse momenta, the underestimation is reduced, but overall the production of J/ψ turns out to be predicted more accurate in comparison to measurements. The statistical uncertainties for ψ(2S) production cross sections are higher in simulation and experiment due to less produced particles per event. However, the deviation does not seem to be a consequence of too few statistics. It is more likely, that there aspects in the PYTHIA physics model which do not describe the real process of ψ(2S) well enough. It is questionable if a new tune on its own can improve the ψ(2S) simulation.

All in all, the very basic trends of charmonium production are predicted by PYTHIA reasonably well. However, the quantitative results partially deviate very much from experimental results. The used *Monash 2013 tune* was created with measurements of up to $\sqrt{s} = 8\,\mathrm{TeV}$, because no particle accelerators were capable of reaching $\sqrt{s} = 13\,\mathrm{TeV}$ at that time. A new tune of the parameters based on $\sqrt{s} = 13\,\mathrm{TeV}$ LHC measurements could possibly improve the charmonium production in PYTHIA. But based on the observations for non-prompt J/ψ, it is also possible that just a new tune on its own may not be capable of simulating charmonium production correctly and an improvement on the implemented physics processes themselves has to be made.

A Appendix

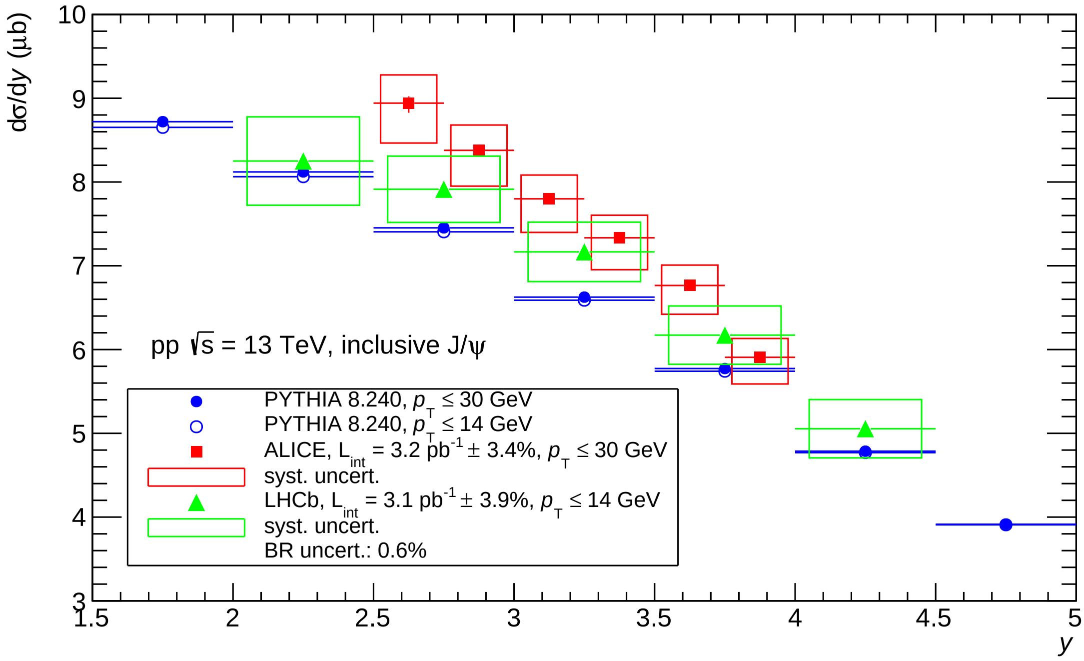

Figure A.1: y-differential inclusive J/ψ cross section at $\sqrt{s} = 13\,\text{TeV}$. The results are compared to ALICE and LHCb data. The plot is zoomed to the rapidity range of the experiments.

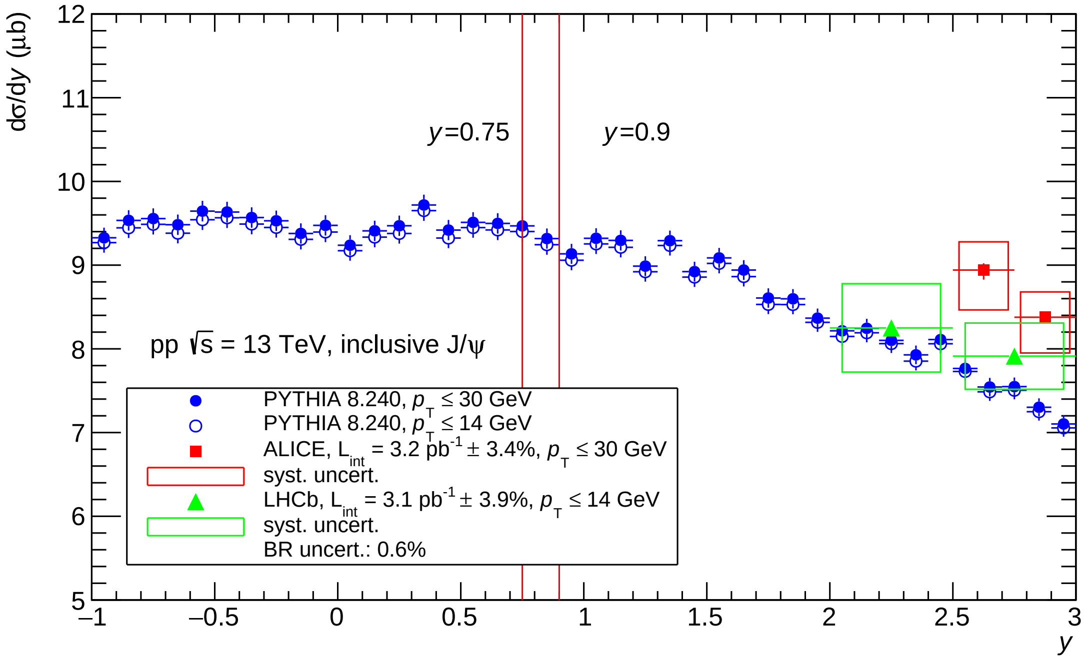

Figure A.2: y-differential inclusive J/ψ cross section at $\sqrt{s} = 13\,\text{TeV}$. The results are compared to ALICE and LHCb data. The plot is zoomed to the rapidity range of the experiments. The plot is zoomed and the data is not rebinned with respect to the PYTHIA-internal bins

Bibliography

[Aab+18] M. Aaboud et al. (ATLAS collaboration). “Measurement of quarkonium production in proton–lead and proton–proton collisions at 5.02 TeV with the ATLAS detector”. In: *The European Physical Journal C* 78.3 (Feb. 2018). URL: `http://dx.doi.org/10.1140/epjc/s10052-018-5624-4`.

[Aai+15] R. Aaij et al. (LHCb collaboration). “Measurement of forward J/ψ production cross-sections in *pp* collisions at $\sqrt{s}$ = 13 TeV”. In: *Journal of High Energy Physics* 2015.10 (Oct. 2015). URL: `http://dx.doi.org/10.1007/JHEP10(2015)172`.

[Aam+08] K. Aamodt et al. (ALICE collaboration). “The ALICE experiment at the CERN LHC”. In: *Journal of Instrumentation* 3.08 (Aug. 2008), S08002–S08002. URL: `https://dx.doi.org/10.1088/1748-0221/3/08/s08002`.

[Ach+17] S. Acharya et al. (ALICE collaboration). “Energy dependence of forward-rapidity J/ψ and ψ(2S) production in *pp* collisions at the LHC”. In: *The European Physical Journal C* 77.6 (June 2017). URL: `http://dx.doi.org/10.1140/epjc/s10052-017-4940-4`.

[Ach+19] S. Acharya et al. (ALICE collaboration). “Inclusive J/ψ production at midrapidity in *pp* collisions at $\sqrt{s} = 5.02$ TeV”. In: *Journal of High Energy Physics* 2019.10 (Oct. 2019). URL: `http://dx.doi.org/10.1007/JHEP10(2019)084`.

[BC03] L. Betev and P. Chochula (ALICE collaboration). *Definition of the ALICE Coordinate System and Basic Rules for Subdetector Components Numbering*. Last downloaded 07.09.2020. 2003. URL: `http://personalpages.to.infn.it/~tosello/EngMeet/NamingConventions/ALICE-INT-2003-038.pdf`.

[Cac+12] M. Cacciari et al. “Theoretical predictions for charm and bottom production at the LHC”. In: *Journal of High Energy Physics* 2012.10 (Oct. 2012). URL: `http://dx.doi.org/10.1007/JHEP10(2012)137`.

[CER17] CERN. *LHC - The Guide*. Last downloaded 07.09.2020. 2017. URL: `http://press.cern/press-kit`.

[CER20] CERN. *High-Luminosity LHC*. Last downloaded 08.09.2020. 2020. URL: https://home.cern/science/accelerators/high-luminosity-lhc.

[CGN98] M. Cacciari, M. Greco, and P. Nason. "The p_T spectrum in heavy-flavour hadroproduction". In: *Journal of High Energy Physics* 1998.05 (May 1998), pp. 007–007. URL: https://dx.doi.org/10.1088%2F1126-6708%2F1998%2F05%2F007.

[Dem17] W. Demtröder. *Experimentalphysik 4: Kern-, Teilchen- und Astrophysik*. Springer-Lehrbuch. Springer Berlin Heidelberg, 2017. URL: https://dx.doi.org/10.1007/978-3-662-52884-6.

[Mis19] MissMJ, Cush. *File:Standard Model of Elementary Particles.svg*. Last downloaded 17.09.2020. 2019. URL: https://en.wikipedia.org/wiki/File:Standard_Model_of_Elementary_Particles.svg.

[Mob16] Esma Mobs. *The CERN accelerator complex. Complexe des accélérateurs du CERN*. July 2016. URL: http://cds.cern.ch/record/2197559.

[Pov+14] Bogdan Povh et al. *Teilchen und Kerne*. Springer Spektrum. Springer Berlin Heidelberg, 2014. URL: https://dx.doi.org/10.1007/978-3-642-37822-5.

[SCR14] P. Skands, S. Carrazza, and J. Rojo. "Tuning PYTHIA 8.1: the Monash 2013 tune". In: *The European Physical Journal C* 74.8 (Aug. 2014). URL: http://dx.doi.org/10.1140/epjc/s10052-014-3024-y.

[Sjö+15] Torbjörn Sjöstrand et al. "An introduction to PYTHIA 8.2". In: *Computer Physics Communications* 191 (June 2015), pp. 159–177. URL: http://dx.doi.org/10.1016/j.cpc.2015.01.024.

[SR11] Johanna Stachel and Klaus Reygers. *QGP Physics - from Fixed Target to LHC: 2. Kinematic Variables*. Last downloaded 25.09.2020. 2011. URL: https://www.physi.uni-heidelberg.de/~reygers/lectures/2011/qgp/qgp_02_kinematics.pdf.

[Tan+18] M. Tanabashi et al. (Particle Data Group). "Review of Particle Physics". In: *Phys. Rev. D* 98.3 (2018), p. 030001. URL: http://dx.doi.org/10.1103/PhysRevD.98.030001.

[Tho09] Mark Thomson. *Handout 8: Quantum Chromodynamics*. Last downloaded 25.09.2020. 2009. URL: https://www.hep.phy.cam.ac.uk/~thomson/lectures/partIIIparticles/Handout8_2009.pdf.